Wind power plants

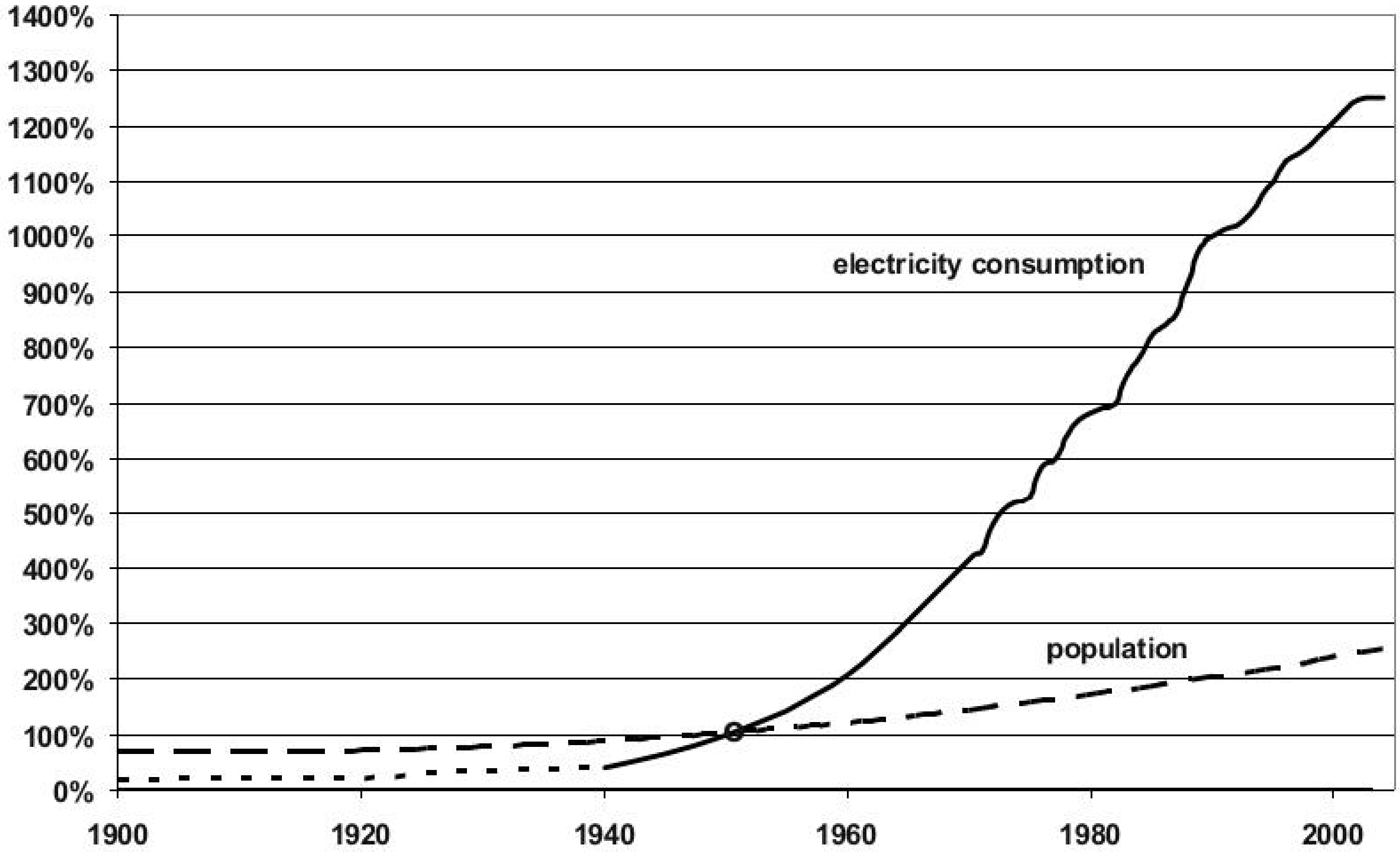

Fig. 1-4 Development of world-wide population and consumption of electricity [3]

1950 = 100%; population = 2.55 10^9; annual electricity consumption = 1.2 10^{12} kWh

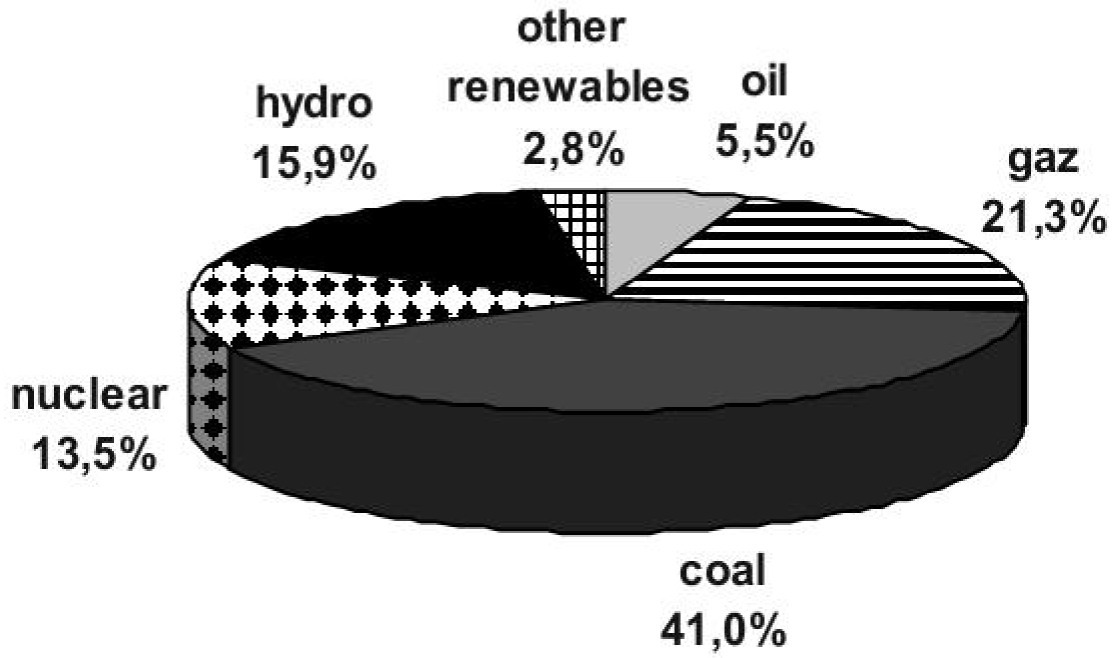

Fig 1-5 Share of the global electricity supply in 2008 [3]

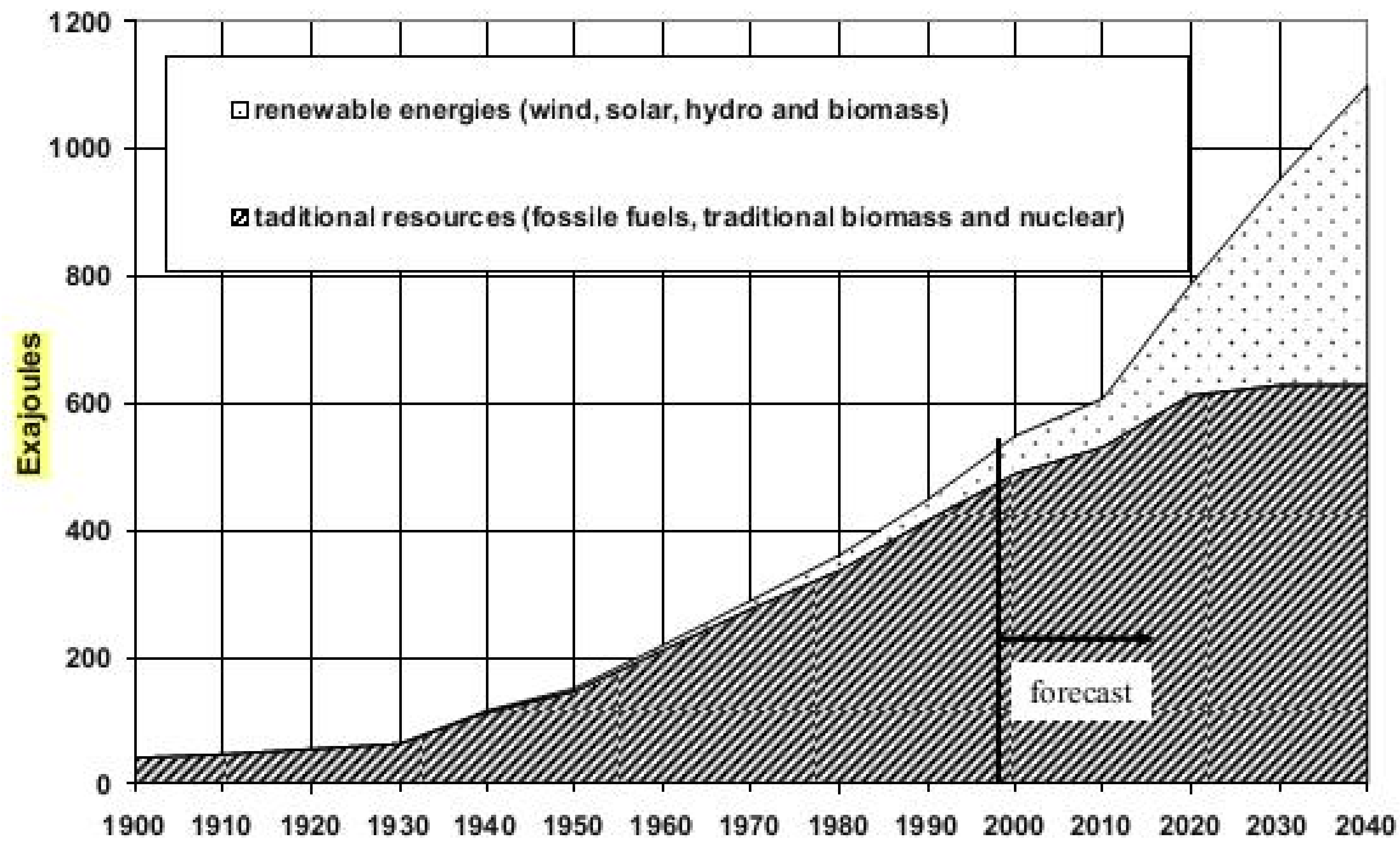

Fig. 1-11 A scenario for meeting future global energy demand [10]

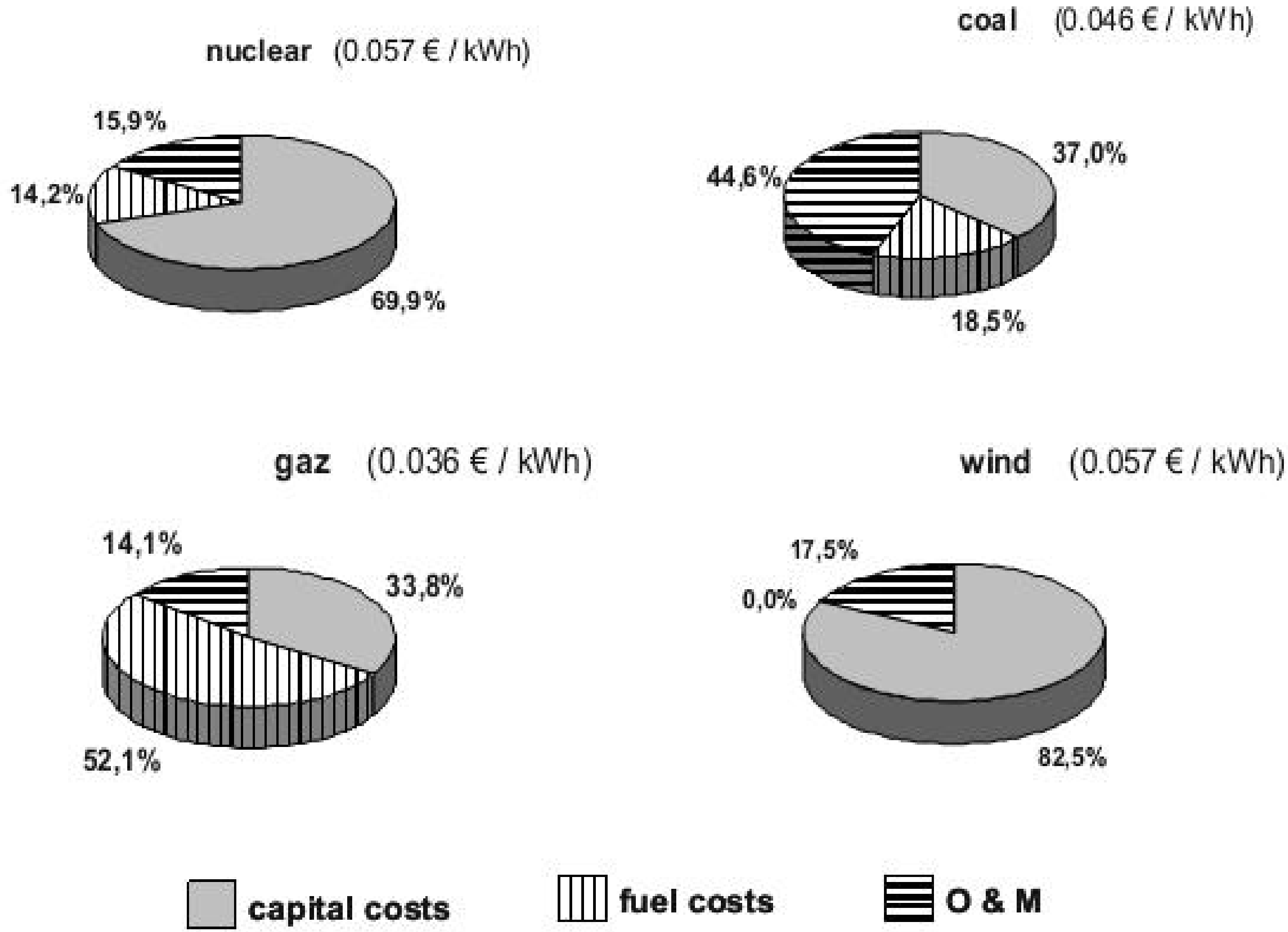

Fig. 1-10 Cost distribution for different power sources [9]

- capital costs - the total upfront investment
- fuel costs
- costs of operation and maintenance (O&M costs)

	Site	Data	
Hydropower	Itaipu, 1985 (Brazil) Spiez, 1986 (Switzerland)	12.600 MW H = 200 m 23 MW H = 65 m	6 W / m^2 70 W / m^2 (per m^2 flooded area)
Brown coal (lignite) fired plants	Schkopau, 1996 (Germany) Schwarze Pumpe, 1998 (Germany) Buschhaus, 1985 (Germany)	1.000 MW 1.600 MW 380 MW	8 W / m^2 16 W / m^2 31 W / m^2 (per m^2 mining area)
Wind power plants	Germany	v_{Wind} = 4.5-6.0 m/s	50 - 120 W / m^2 (per m^2 rotor area) foundation area is 10 times less

Fig. 1-8 Electrical power produced per square meter land use

- renewable energy plants are able to produce enough energy to pay back the amount of energy used to manufacture them. This so-called energy amortisation

	Wind			Solar			Water		
	4.5 m/s	5.5 m/s	6.5 m/s	Mono	Multi	Amorph	Large	Small	Micro
Energy amortisation (in months)	6 - 20	4 - 13	2 - 8	28 - 55	19 - 38	14 - 28	5 - 6	8 - 9	9 - 11

Fig 1-9 Energy amortisation of different renewable energy sources [8]

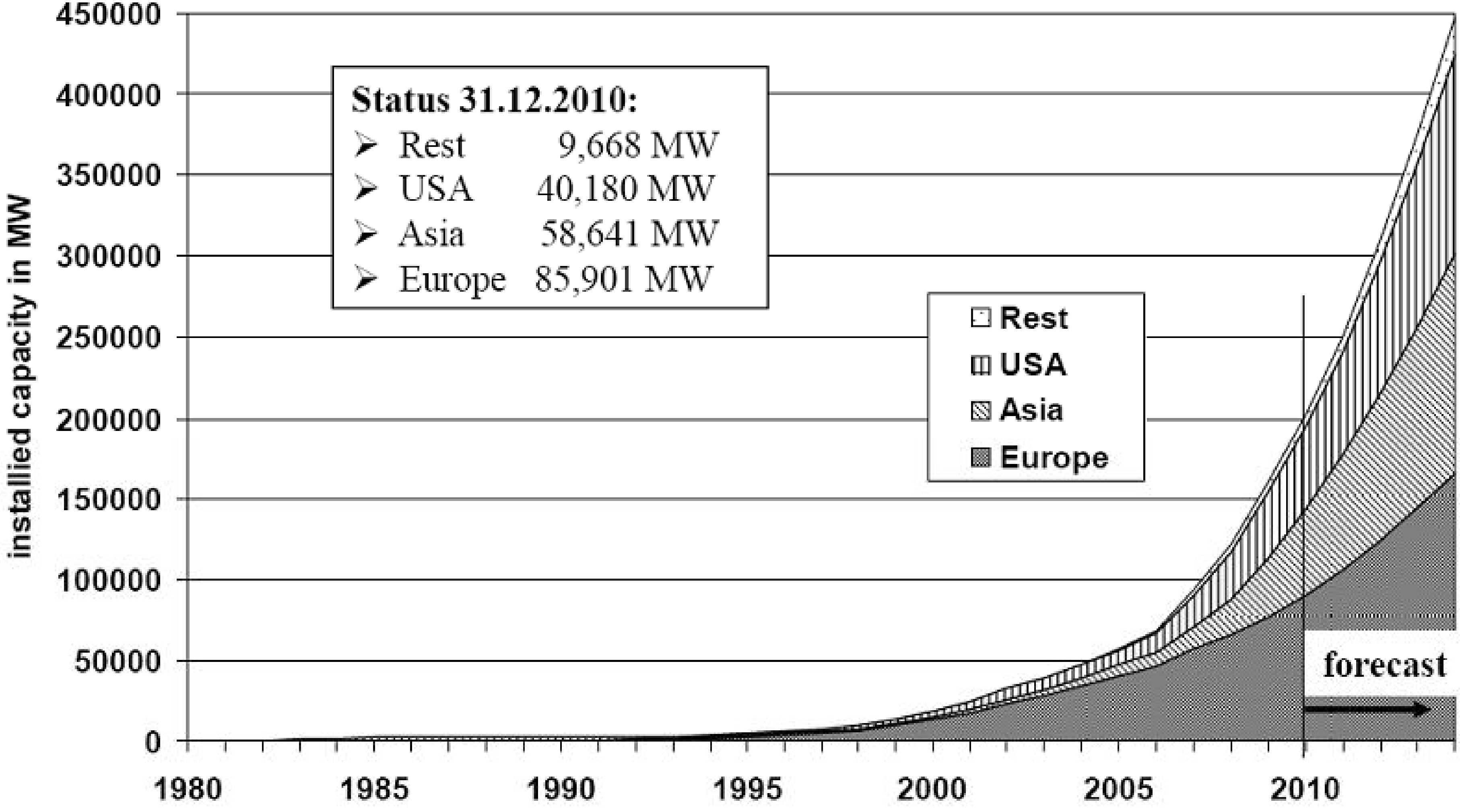

Fig 1-2 Wind energy utilisation, total installed capacity in MW [1, 2]

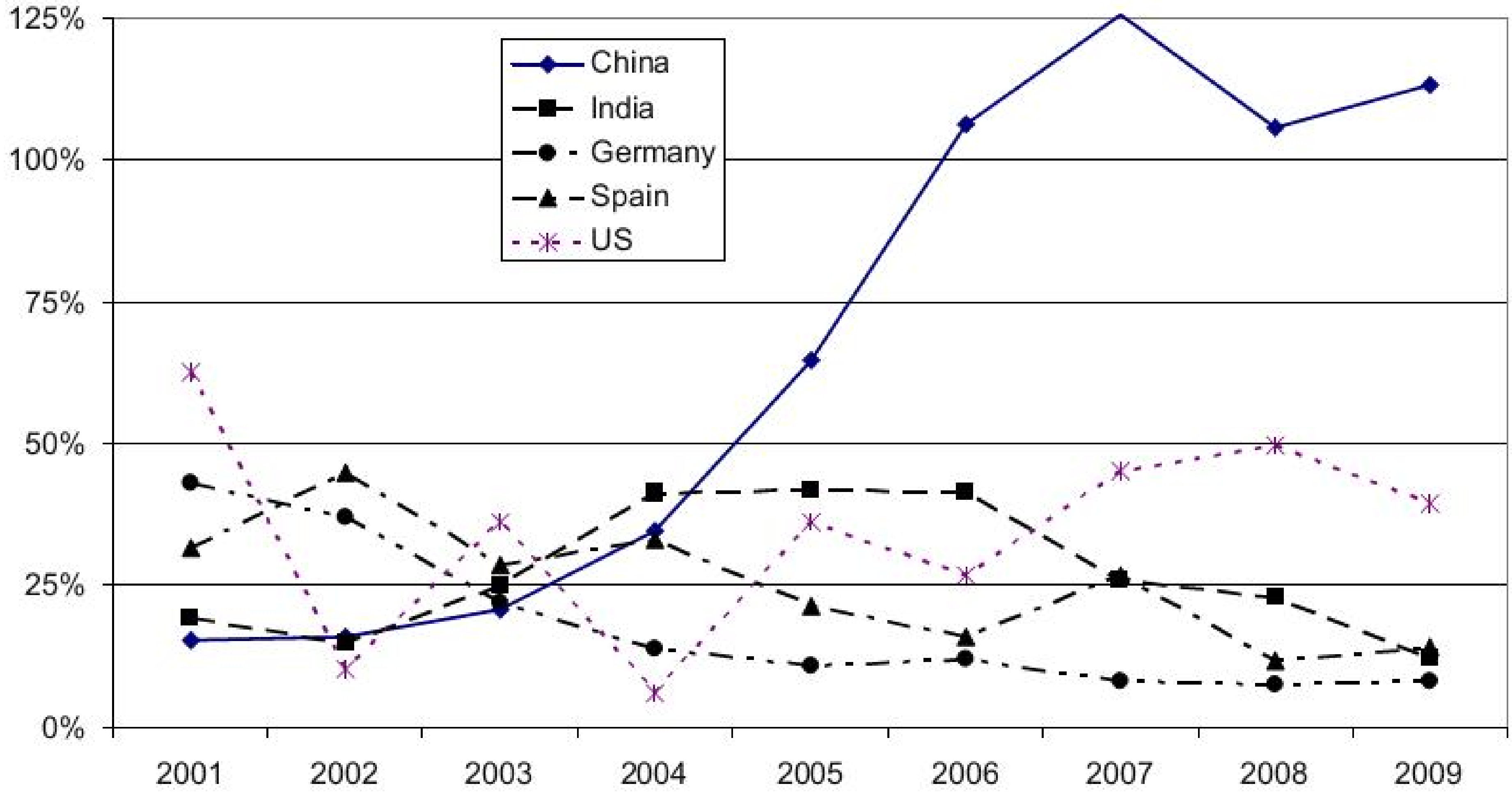

Fig 1-3 Growth rates in top 5 most important markets

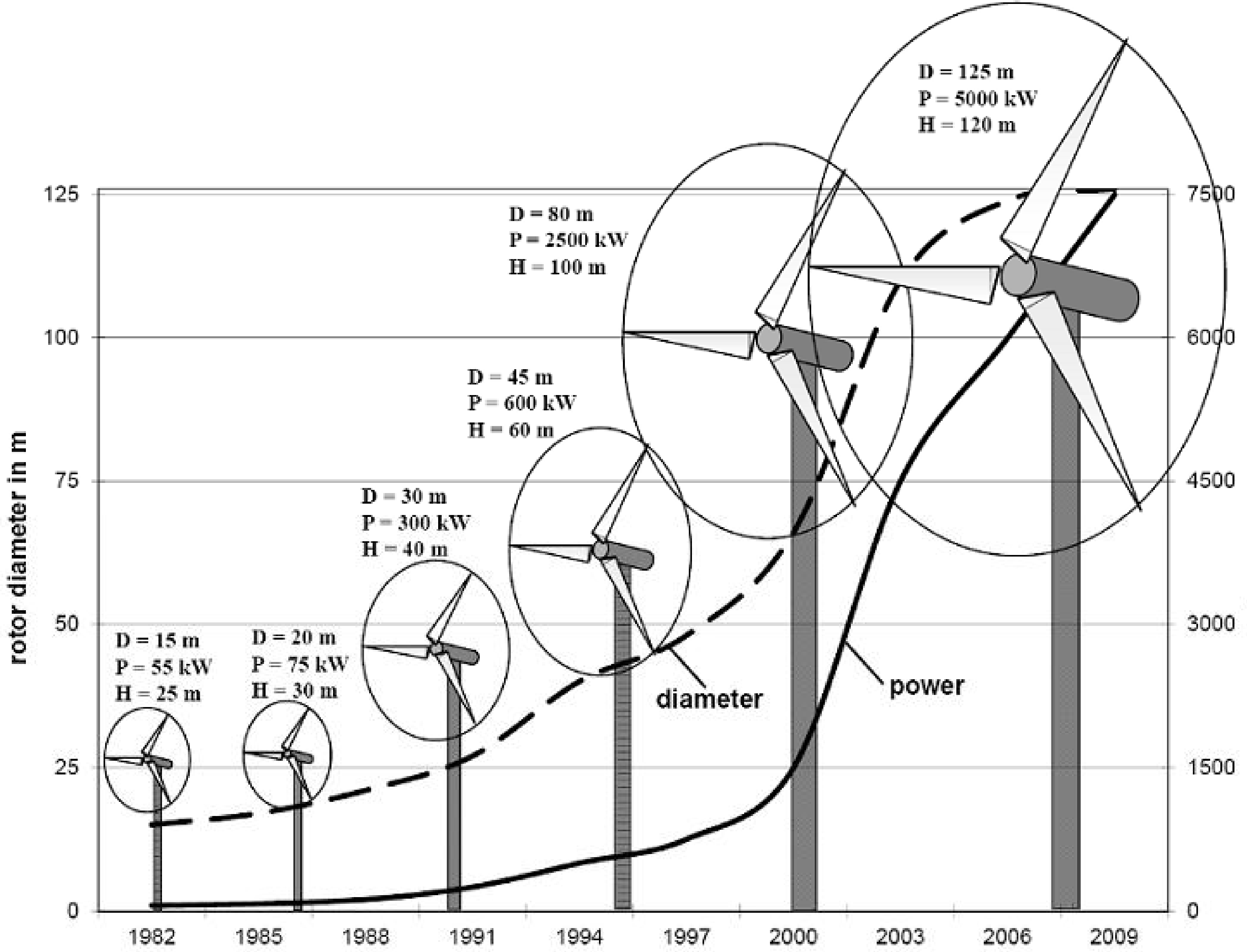

Fig 1-1 Size and power increases of commercially produced wind turbines over time

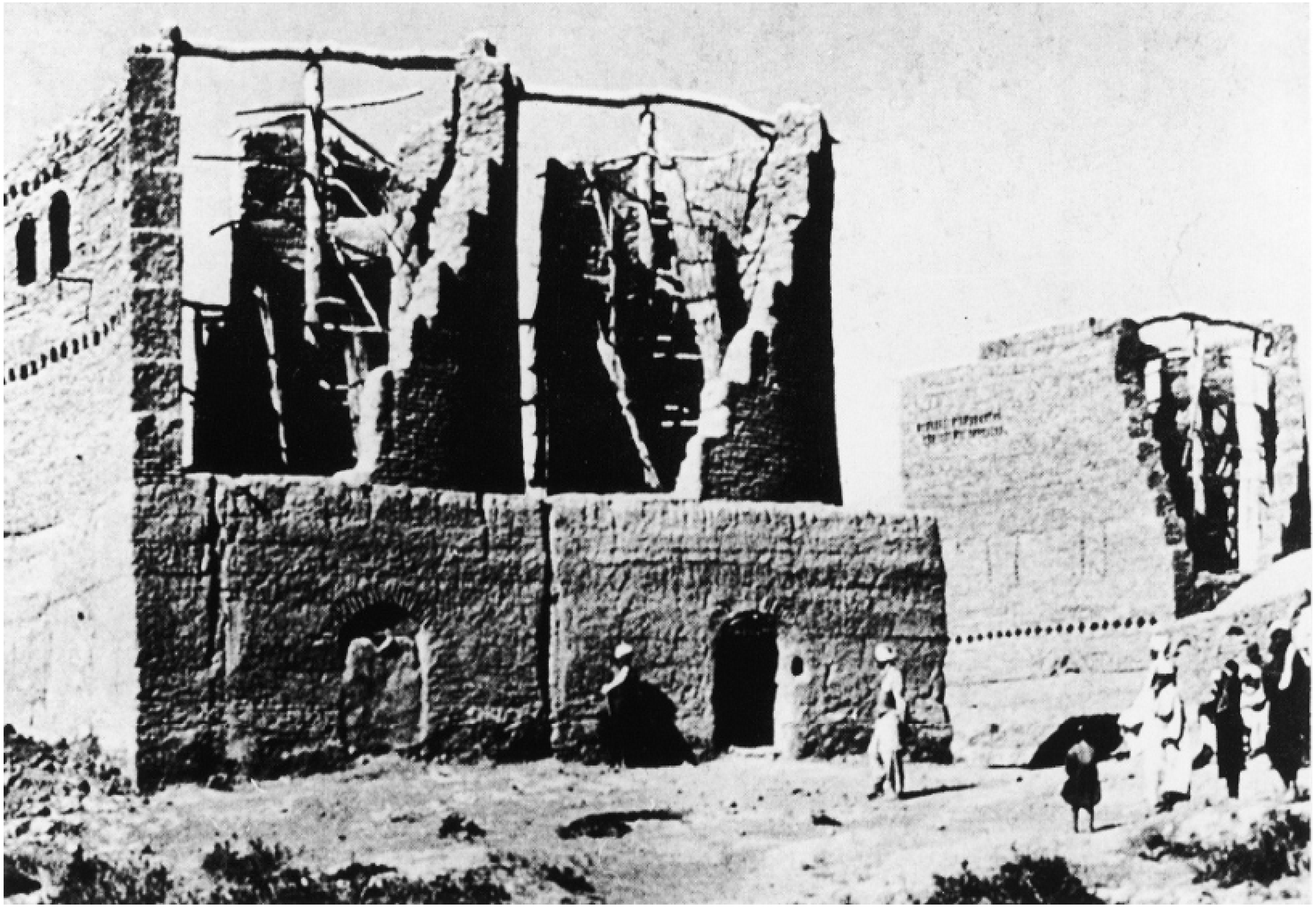

Ruins of a vertical axis windmill in Afghanistan, 1977

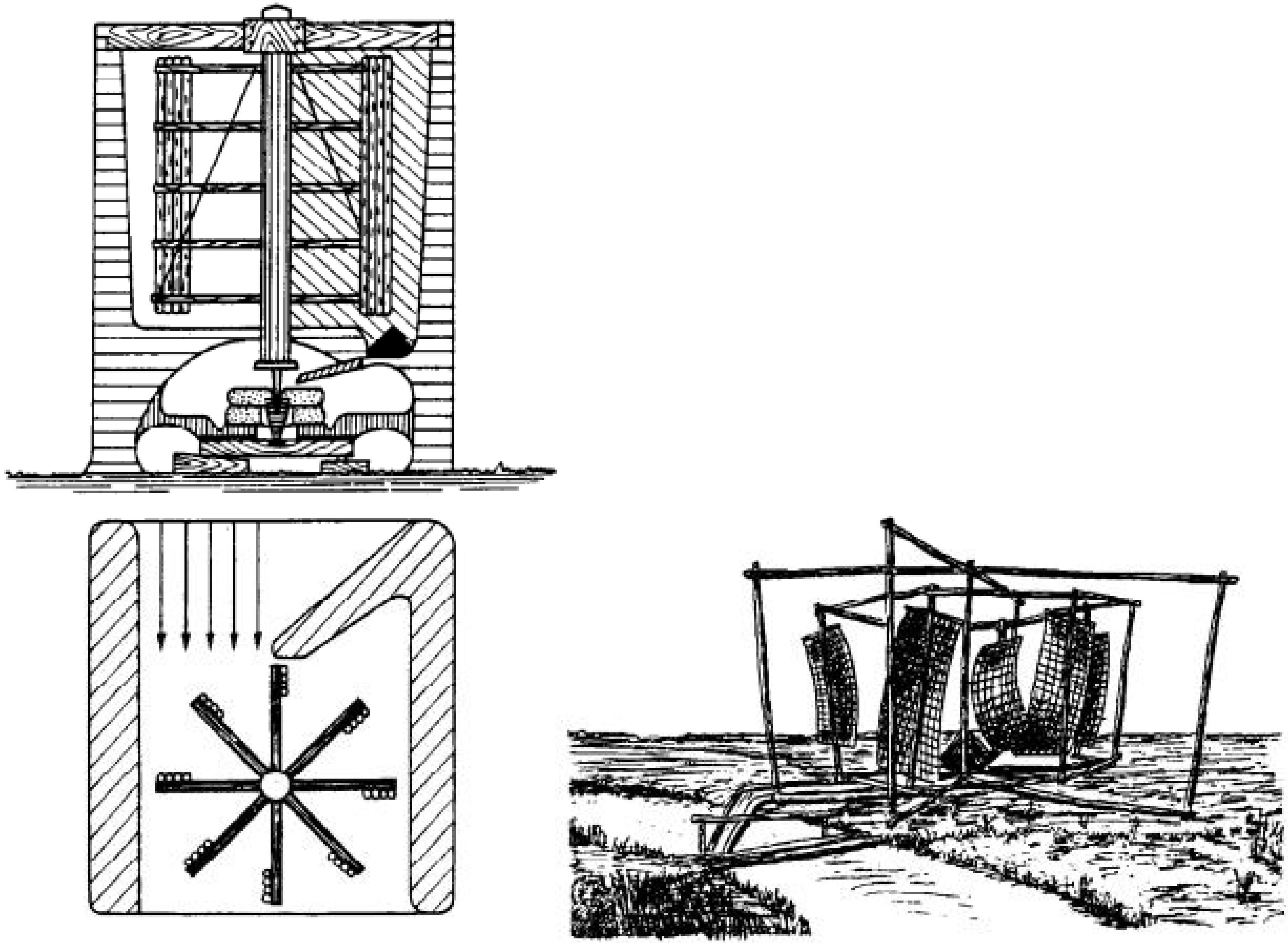

a) b)

Persian windmill [3] b) Chinese windmill with flapping sails

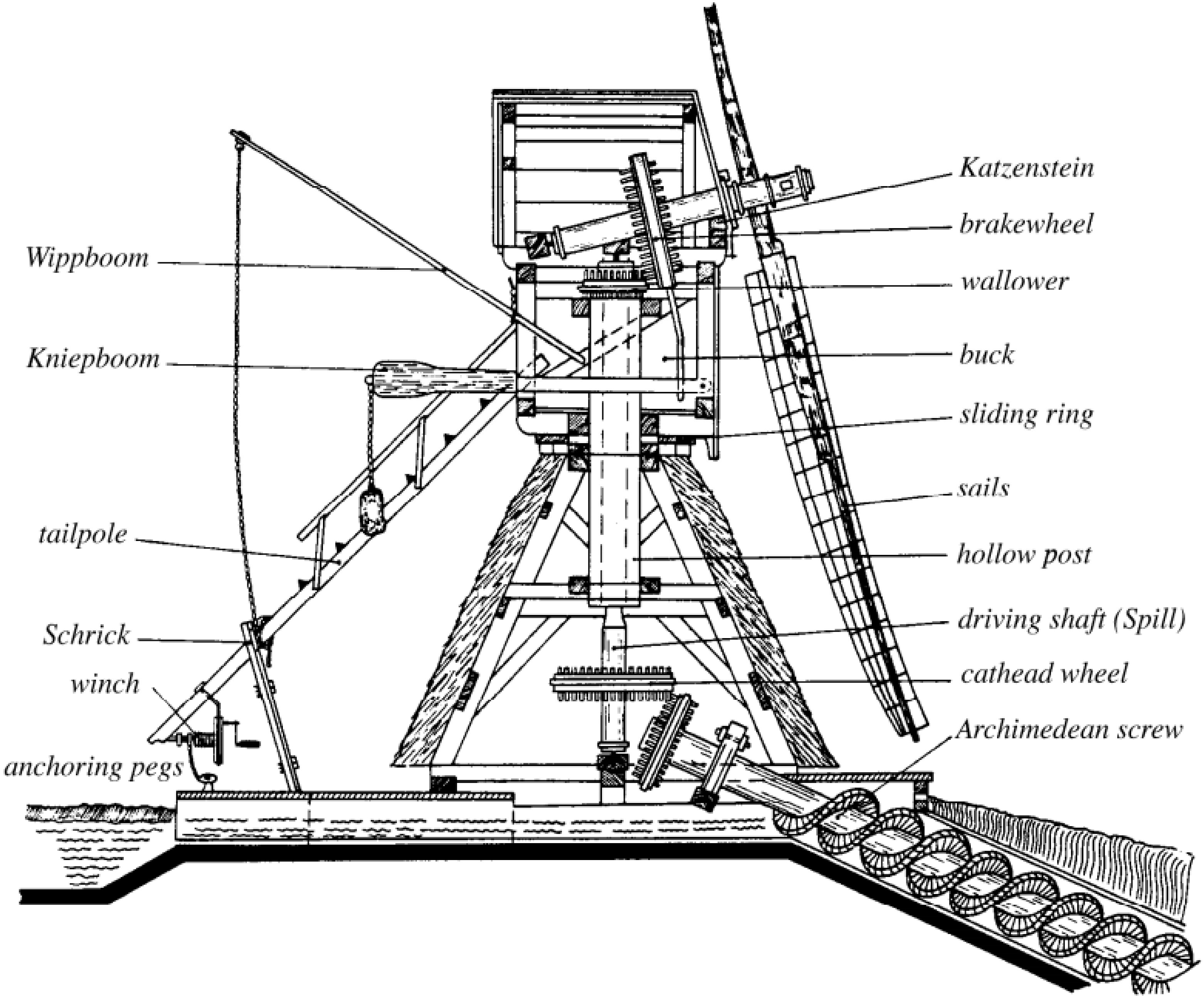
Katzenstein
brakewheel
Wippboom
wallower
Kniepboom
buck
sliding ring
sails
tailpole
hollow post
driving shaft (Spill)
Schrick
cathead wheel
winch
Archimedean screw
anchoring pegs

Vertical and Horizontal axis wind turbines

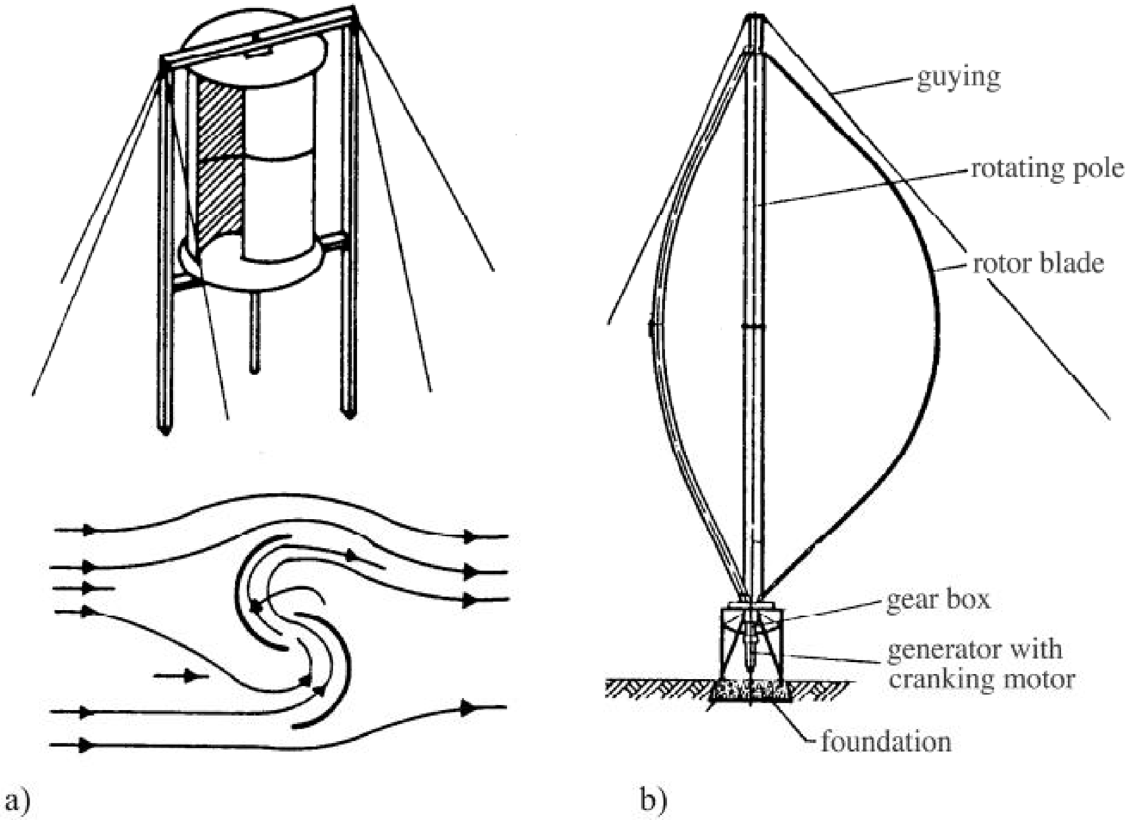

Fig. 2-4 a) Savonius rotor [5]; b) Darrieus rotor [6]

The physics of the use of wind energy

Wind power

air mass

kinetic energy $$E = \frac{1}{2} m v^2$$ velocity

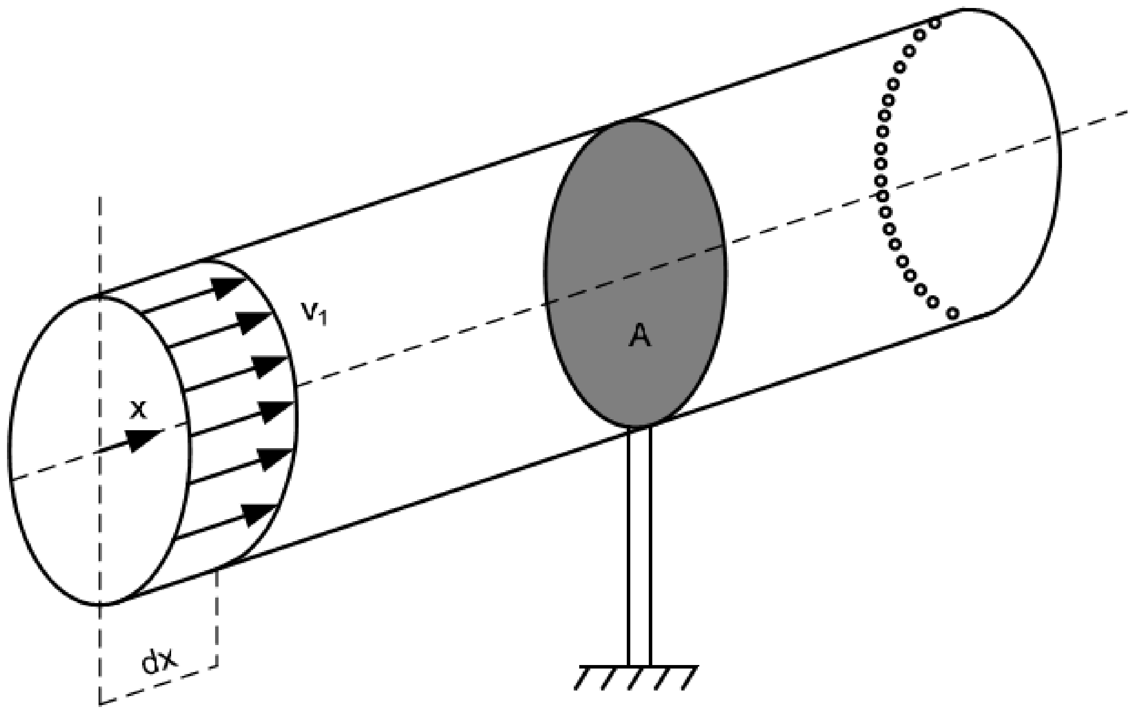

$$\dot{m} = \mathrm{A}\,\rho\,\frac{dx}{dt} = \rho\, A\, v$$

cross sectional area air density

$$P_{\mathrm{wind}} = \dot{E} = \frac{1}{2}\,\dot{m}\,v^2 = \frac{1}{2}\,\rho\,A\,v^3$$

The power of the wind is converted into mechanical power of the rotor by deceleration of the flowing air mass

Betz Law

maximum power is extracted by a free (i.e. unshrouded) wind turbine if the original upstream wind velocity v1 is reduced to a velocity v3= v1/3 far downstream the rotor.

the resulting velocity in the rotor plane $v_2 = 2v_1/3$

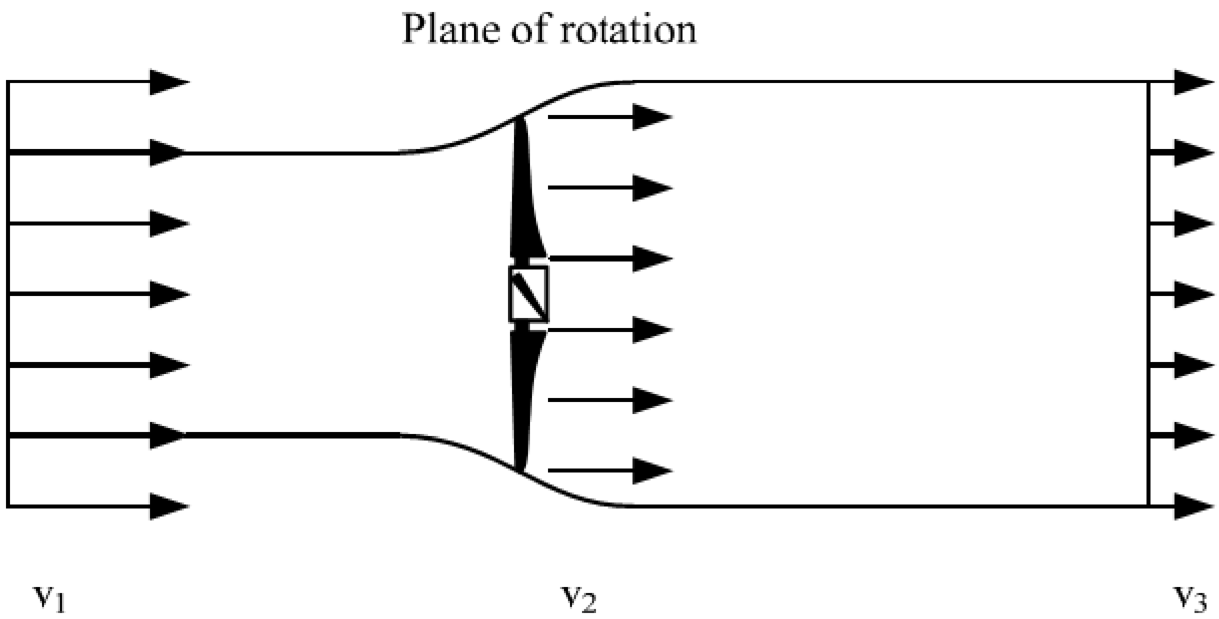

In that case of a theoretically maximum power extraction, the result is

$$P_{\text{Betz}} = \frac{1}{2}\, \rho\, A\, v^3\, c_{\text{P.Betz}}$$

with the maximum power coefficient $c_{\text{P.Betz}} = {}^{16}/_{27} = 0.59$

Even in this best case of power extraction without any losses, only 59 % of the wind power is extractable.

Drag driven rotors

The drag devices utilise the force that acts on an area aperpendicular to the wind direction

$$D = c_{\mathrm{D}} \frac{\rho}{2} a v^2$$

The drag coefficient cD is the proportional constant and describes the „aero-dynamic quality“ of the body:
the higher the aerodynamic quality of a body, the lower is cDand thus the corresponding drag force

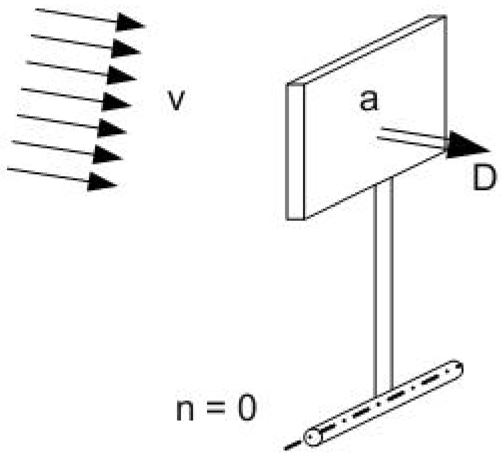

$$D = c_{\mathrm{D}} \frac{\rho}{2} a v^2$$

c_{D}	**Body**
1.11	Circular plate
1.10	Square plate
	Hemisphere
0.33	$\rightarrow$ (open back
1.33	$\rightarrow$) open front

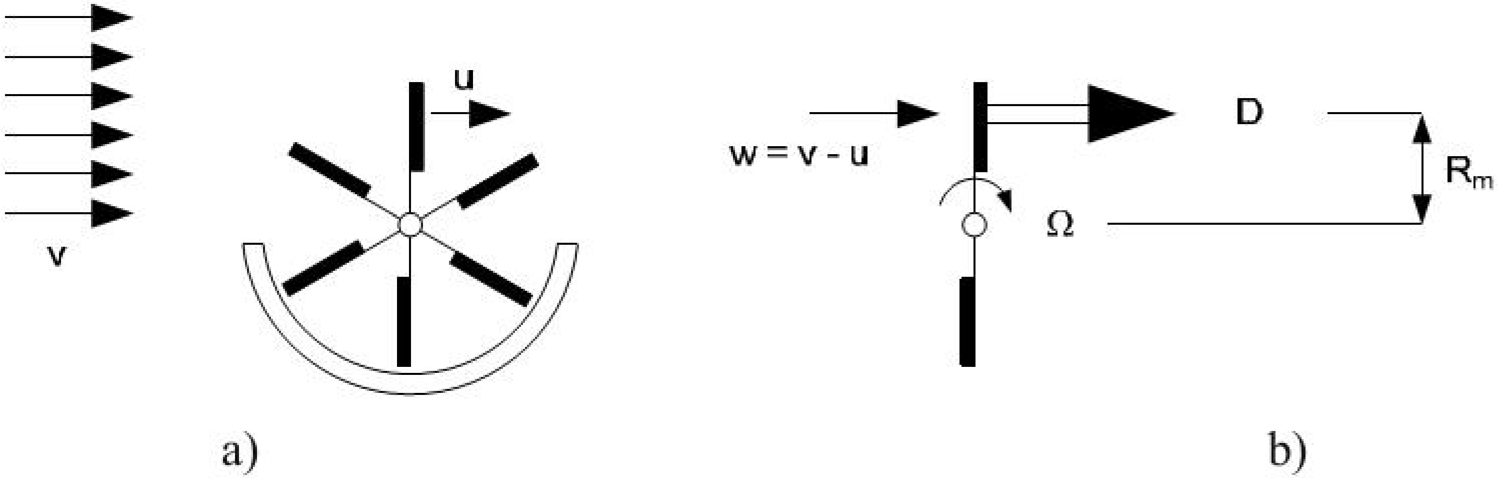

a) Principle of a Persian windmill, b) simplified model

Thus, the resulting drag force on the rotating plate is

$$D = c_{\mathrm{D}} \, \frac{\rho}{2} \, a \, w^2 = c_{\mathrm{D}} \, \frac{\rho}{2} \, a \, (v - u)^2$$

Hence, the mean driving mechanical power – which in reality is slightly pulsating – amounts to

$$P = D\ u = \frac{\rho}{2}\ a\,v^3 \left\{ c_\mathrm{D} \cdot \left(1 - \frac{u}{v}\right)^2 \cdot \frac{u}{v} \right\} = \frac{\rho}{2}\ a\,v^3\, c_\mathrm{P}$$

power coefficient

It gives the portion of the wind power which is converted into mechanical power

the ratio tip speed ratio $\lambda = u \,/\, v$,

$u = \Omega \cdot R_\mathrm{M}$

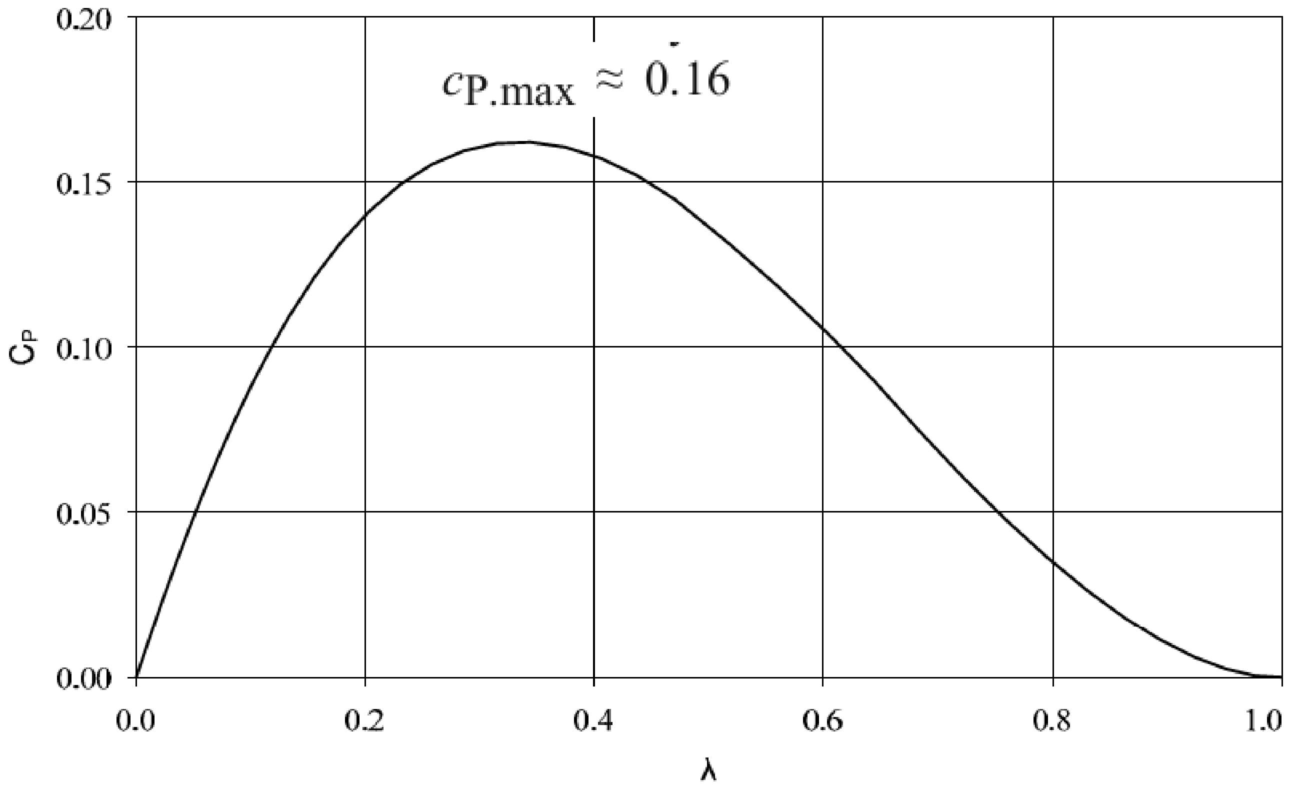

Fig. 2-21 Power coefficient versus tip speed ratio $\lambda = \Omega R_M/v$ of the Persian windmill (approximation for the simplified model)

For a given wind velocity v, the diagram of $c_P(\lambda) = c_P(\Omega \cdot R_M / v)$ shows which portion of the wind power $(\rho/2)\, a\, v^3$ can be extracted

Lift driven rotors

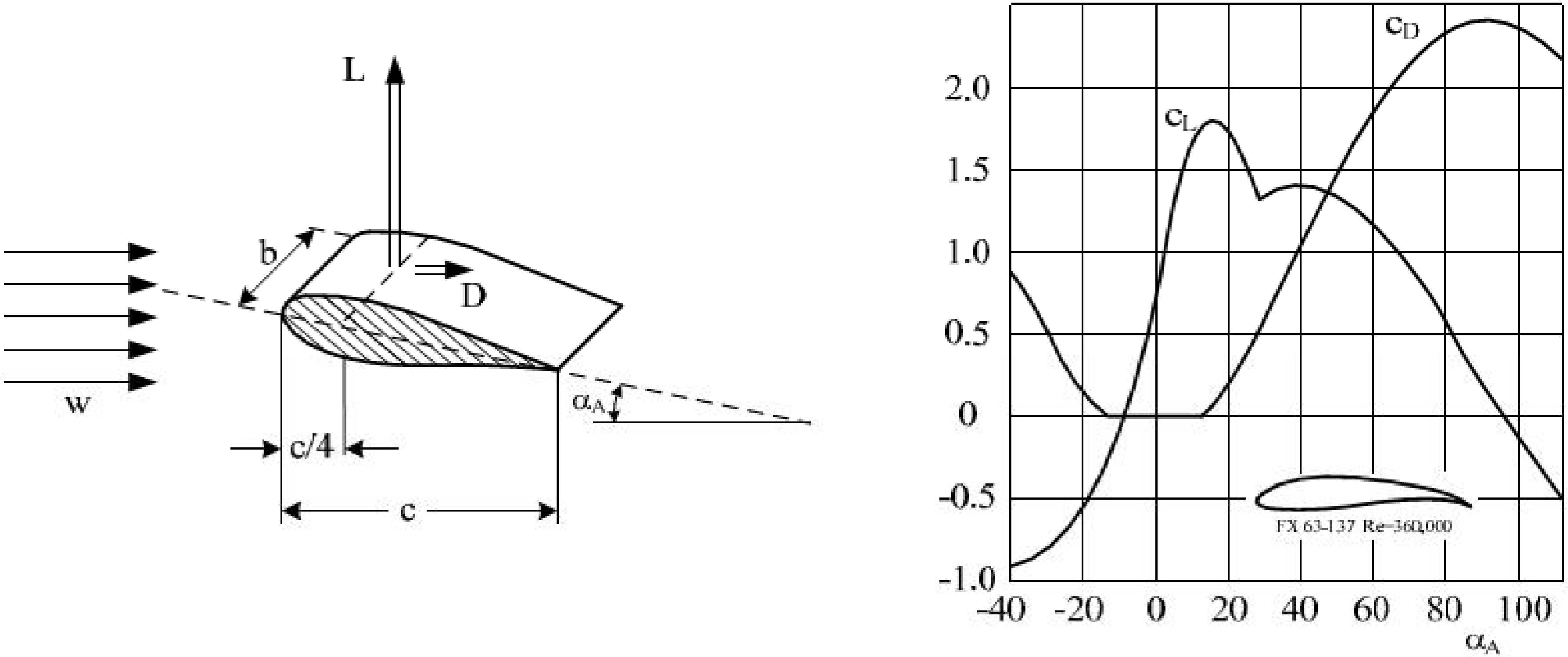

Fig. 2-24 Lift force *L* and drag force *D* of an airfoil and the corresponding coefficients c_L and c_D versus angle of attack α_A

$$L = c_L \frac{\rho}{2} a w^2$$

Similar to the drag force, it is proportional to the projected area $a = c\,b$ and the dynamic pressure $(\rho / 2)\,w^2$. For small angles of attack α_A the lift force L acts at approx. a quarter of the cord length c behind the leading edge.

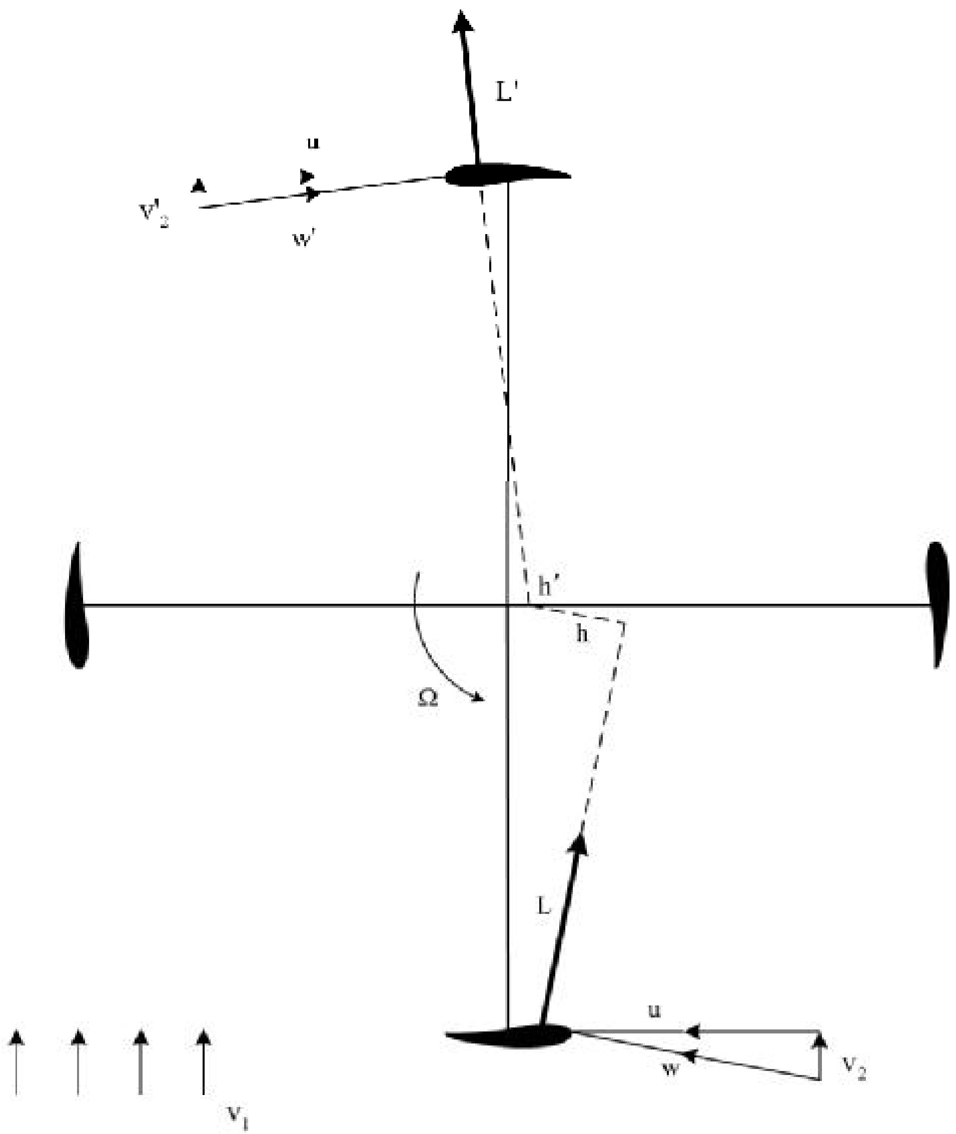

Fig. 2-25 Lift forces L and L' at the Darrieus rotor producing the driving torque

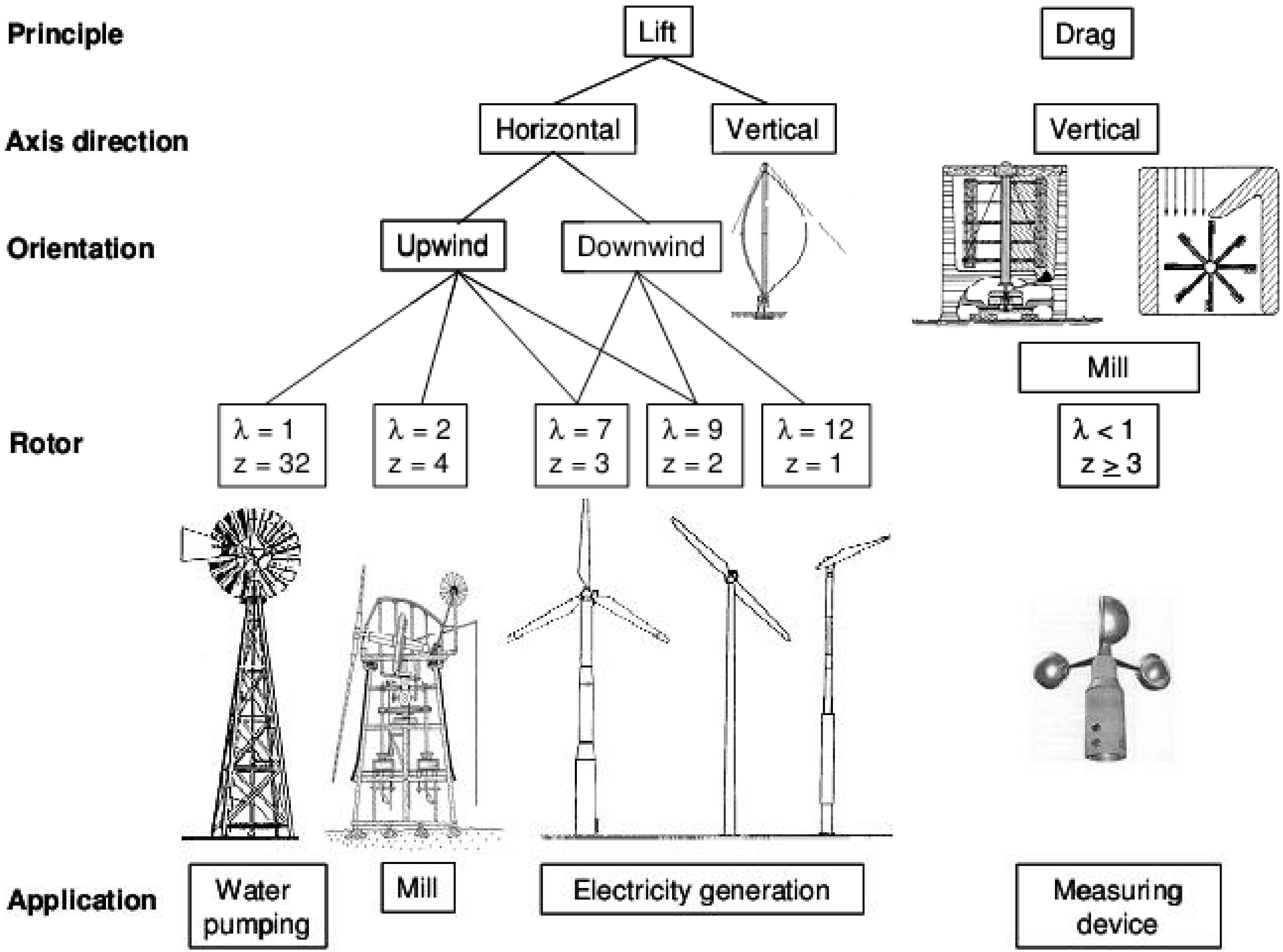

Fig. 3-1 Typology of wind turbines and typical applications

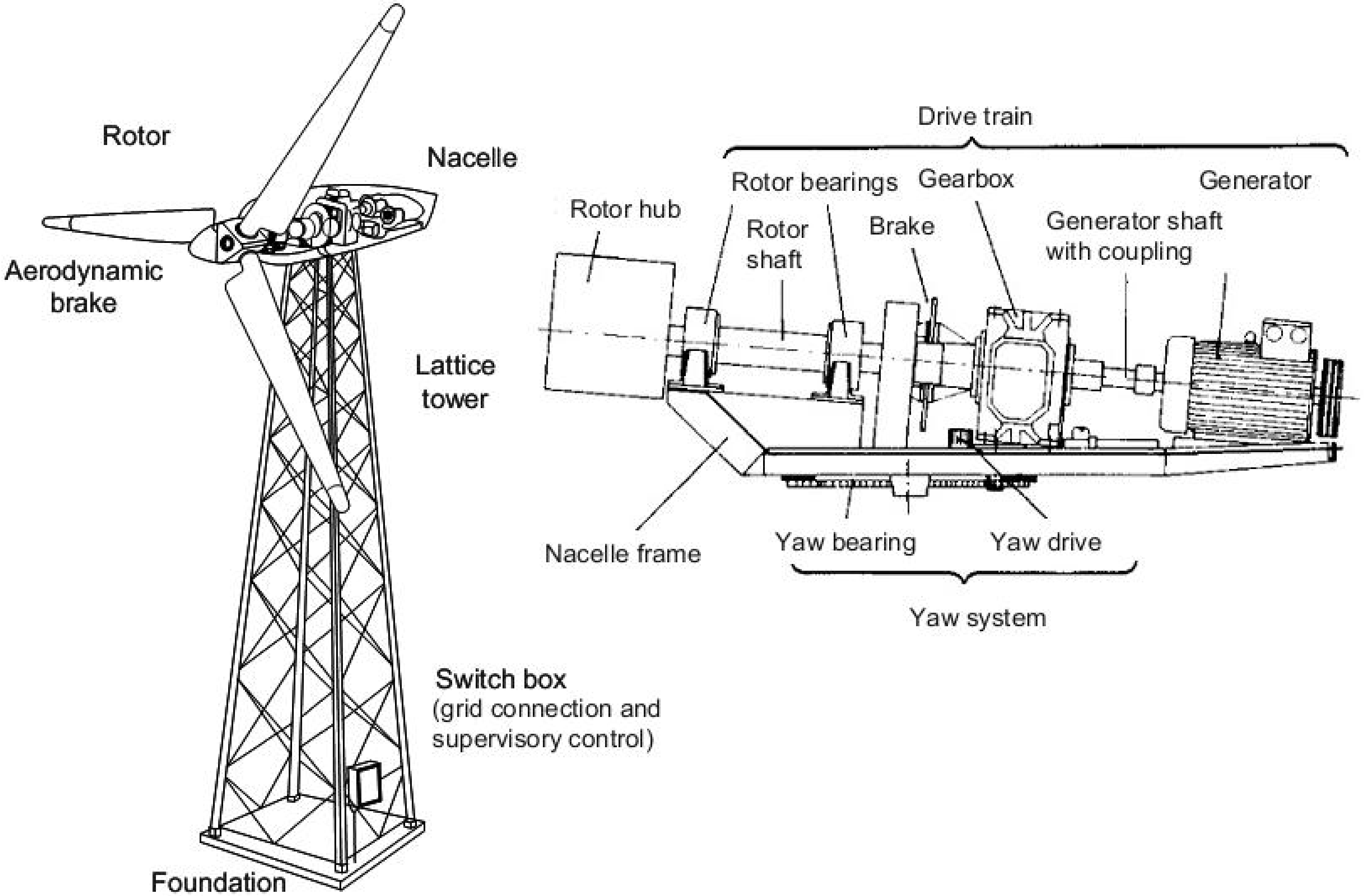

Fig. 3-2 VESTAS V15, general view and nacelle section [1]

Rotor

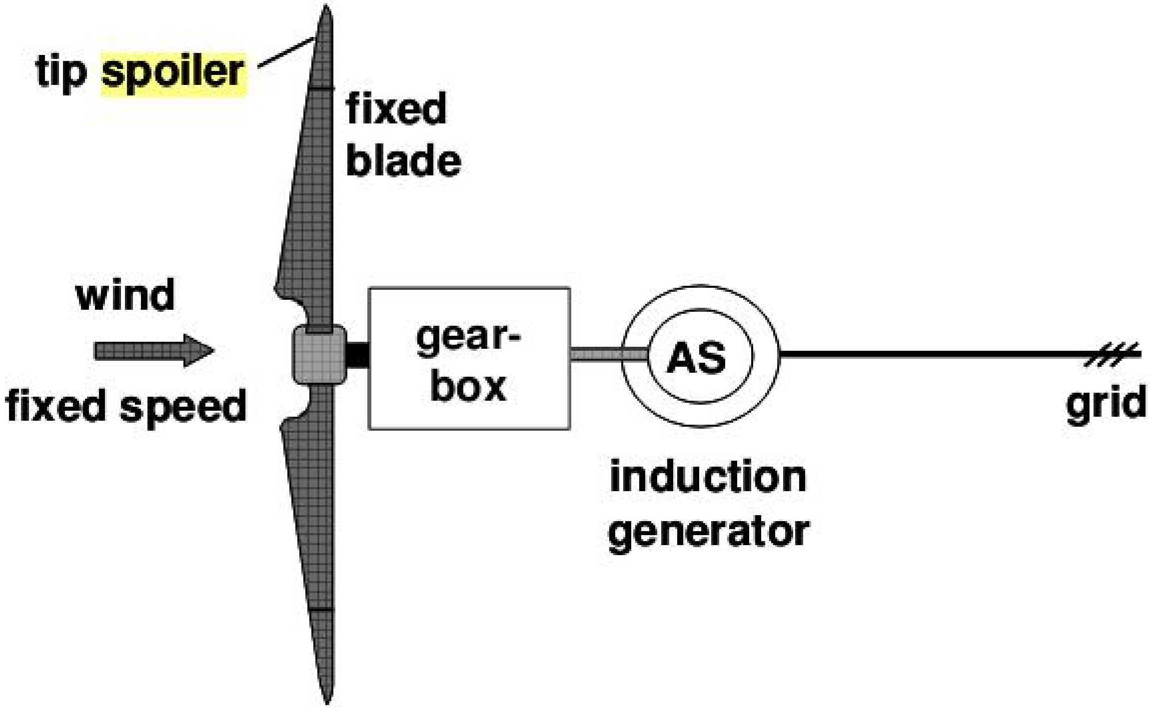

Fig. 1-15 Basic design of a Danish wind turbine with induction generator and constant rotational speed

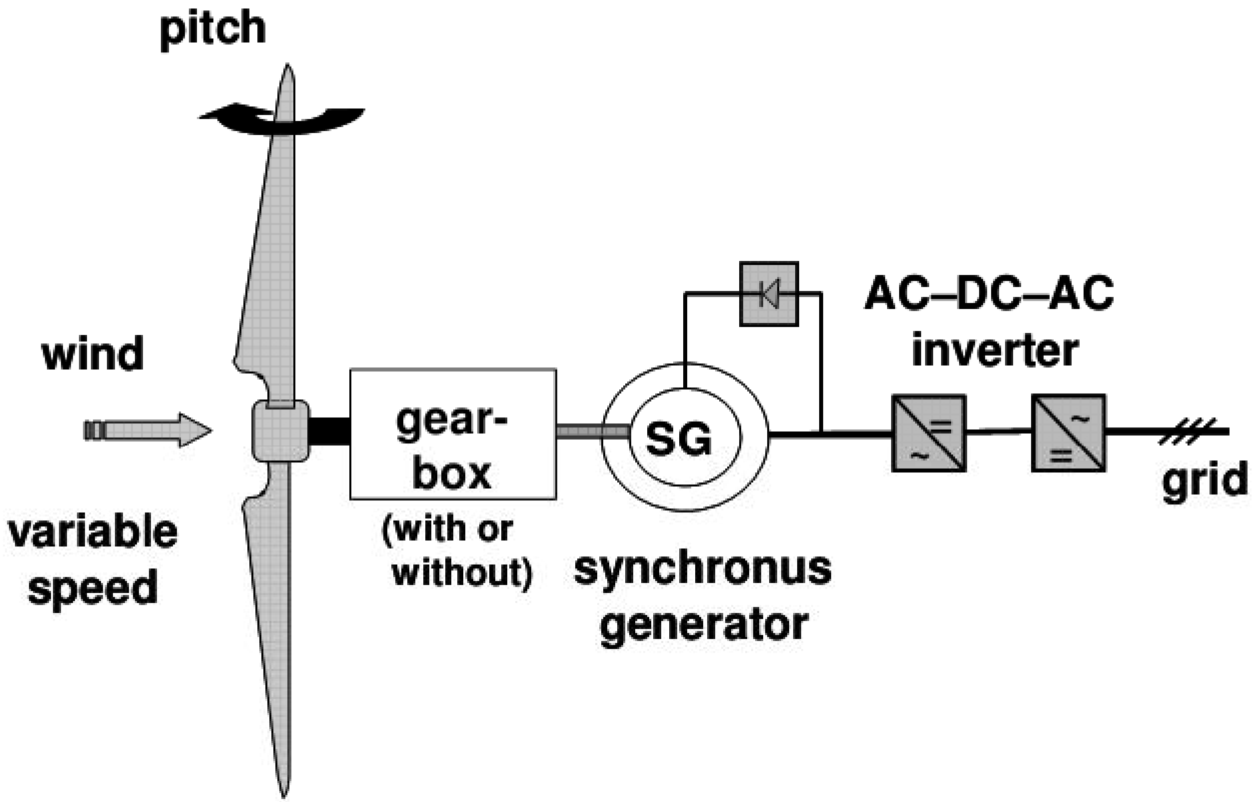

Fig. 1-16 Pitch-controlled variable speed wind turbine with synchronous generator and ac-dc-ac power conversion

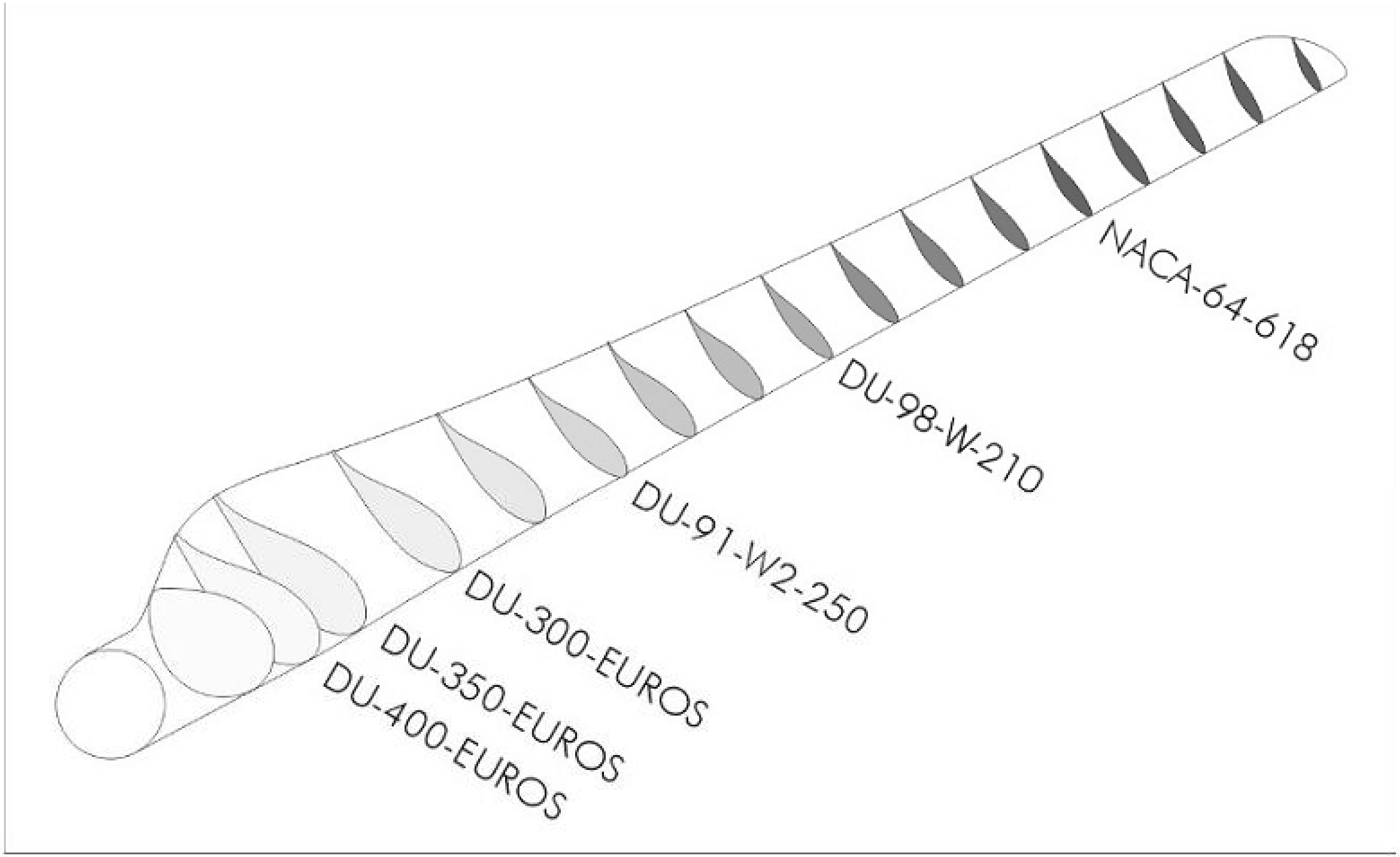

Fig. 3-8 Different blade profiles along the radius of a blade, (EUROS)

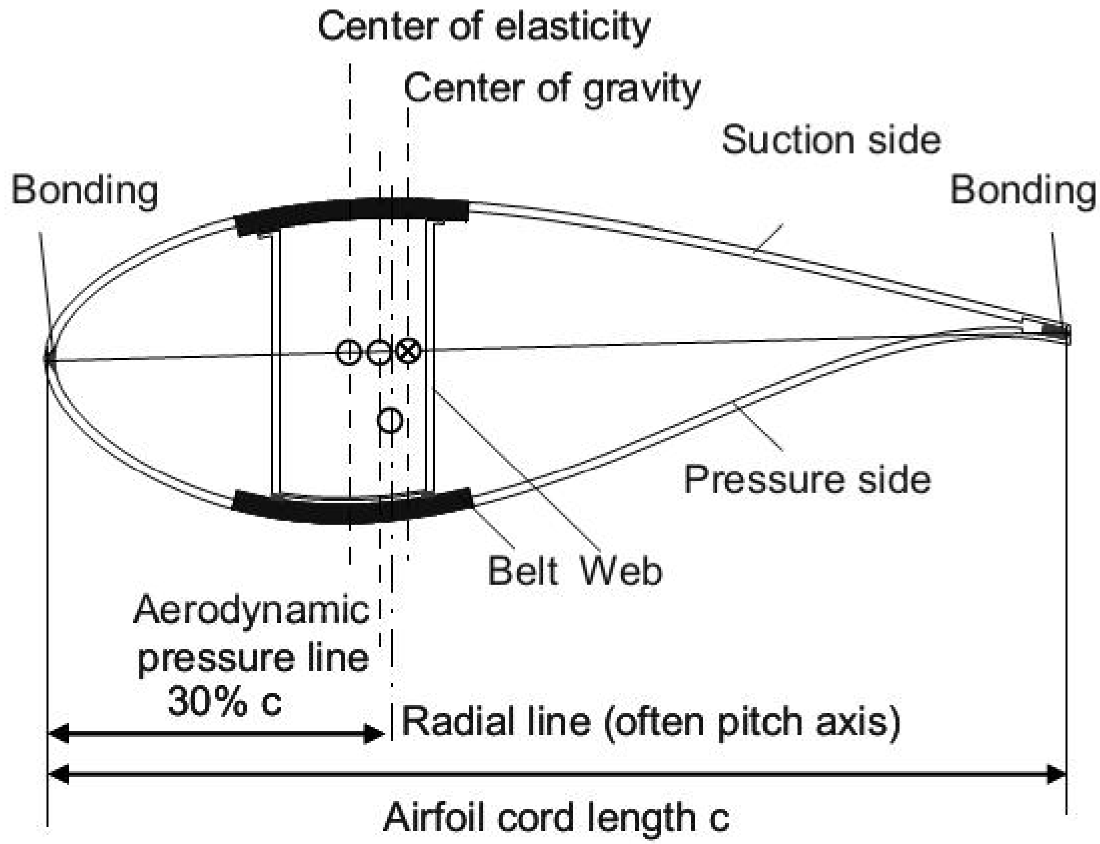

Fig. 3-9 Blade section - characteristic lines of the blade dynamics

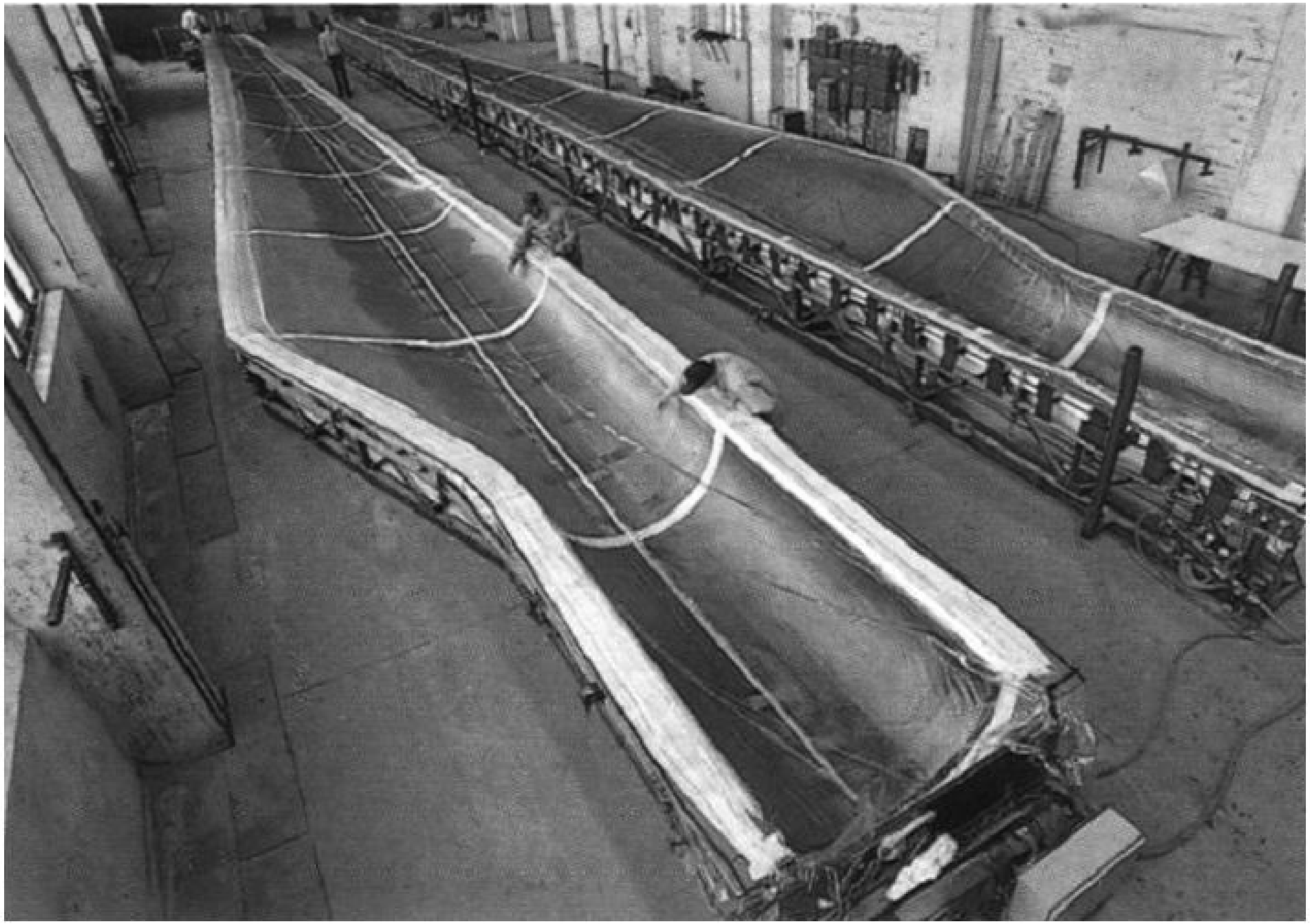

Fig. 3-11 Blade production, separate moulds for suction side and pressure side, mould in front: soaking of the laminate with epoxy resin by a vacuum process (NOI)

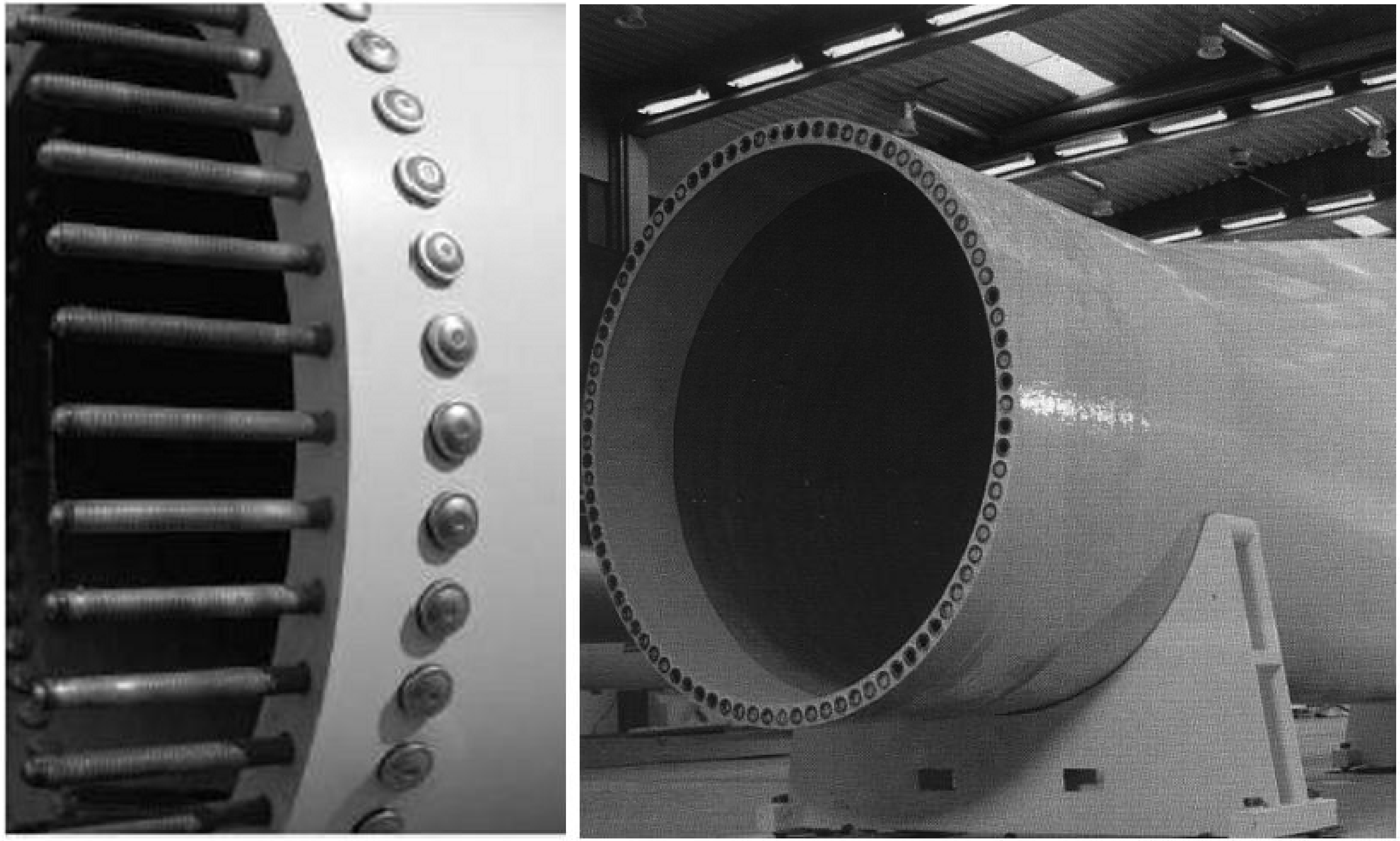

Fig. 3-12 Connection of rotor blade at hub: left “IKEA-bolts” (Bonus), right: bolt sleeves (Vestas)

Hub

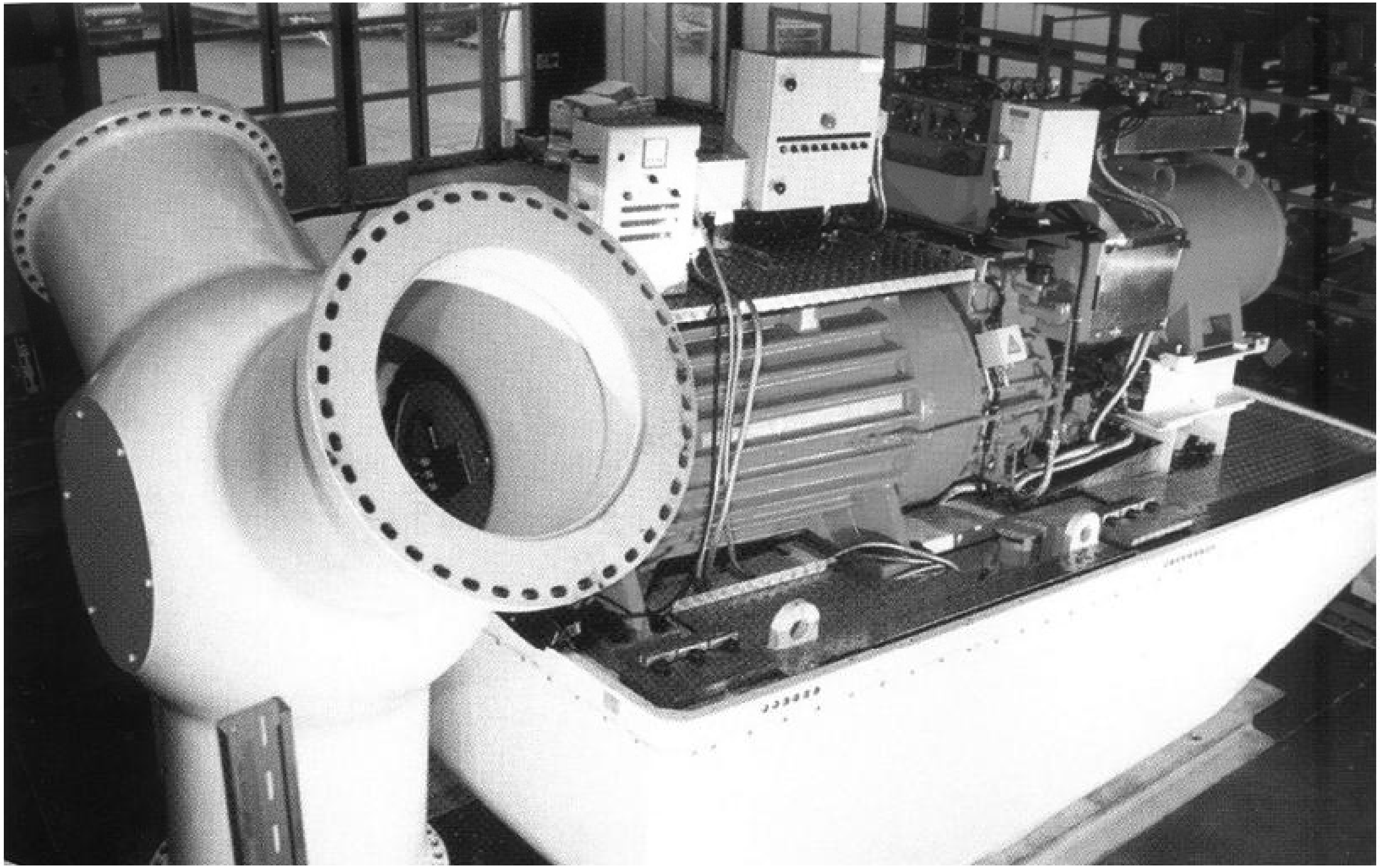

Fig. 3-15 Nacelle with rigid hub of a three-bladed rotor (photo by company Zollern)

Drive train

- the *integrated drive train* where different components with their different functions are fixed directly together and
- the *modular drive train* where most of the components are fixed separately on the nacelle frame.

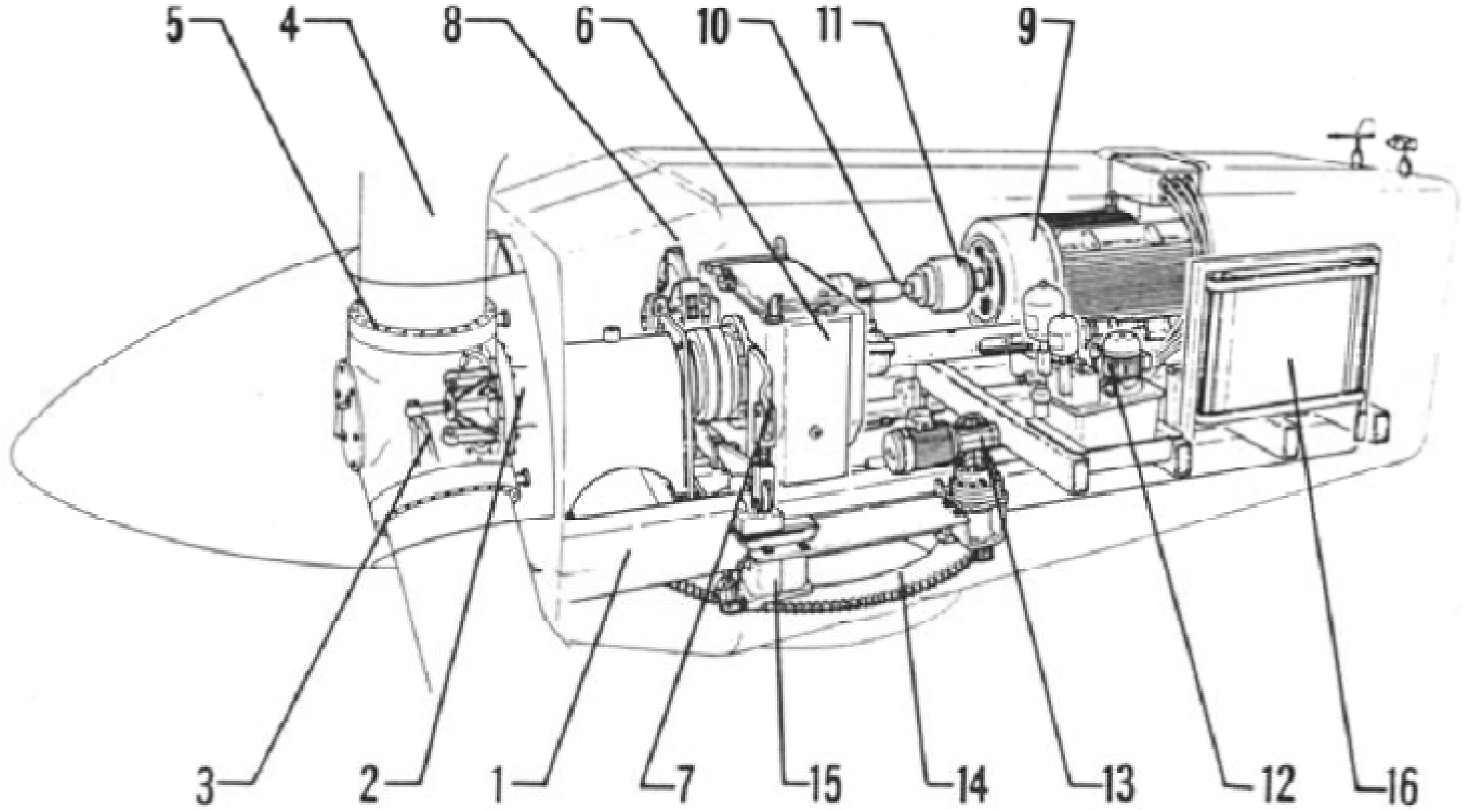

Fig. 3-29 Vestas V27-225, modular drive train; 1 nacelle frame, 2 main shaft, 3 pitch mechanism, 4 rotor blade, 5 cast steel hub, 6 spur gearbox, 7 torsionally elastic gear suspension, 8 brake, 9 pole-switchable asynchronous generator, 10 fast shaft with coupling, 11sliding clutch, 12 hydraulic unit, 13 yaw drive, 14 yaw ring, 15 power cable twist control, 16 top control unit

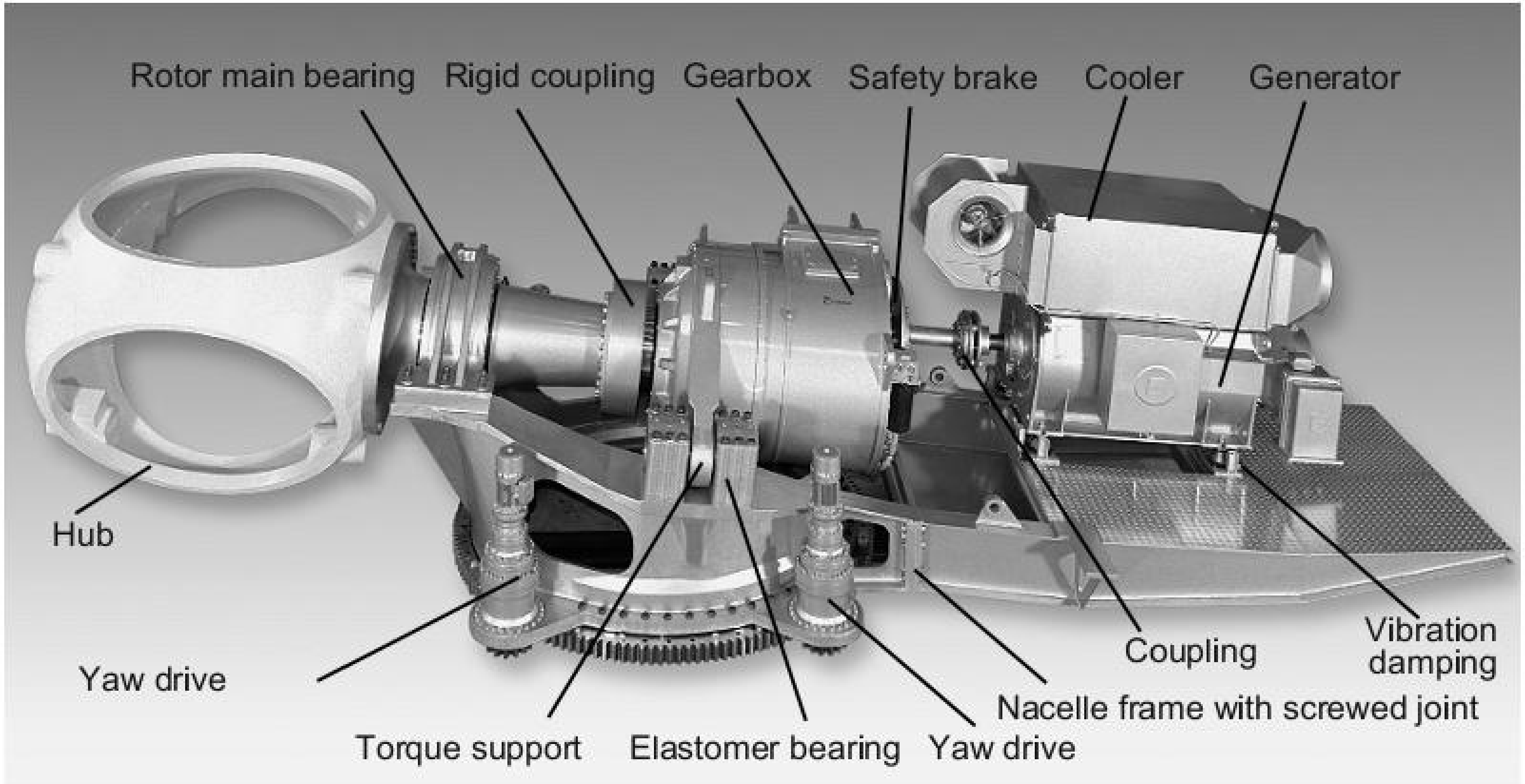

Fig. 3-36 D8, partially integrated drive train design with split, cast nacelle frame and main shaft supported at three points (DeWind 2002)

Gearbox

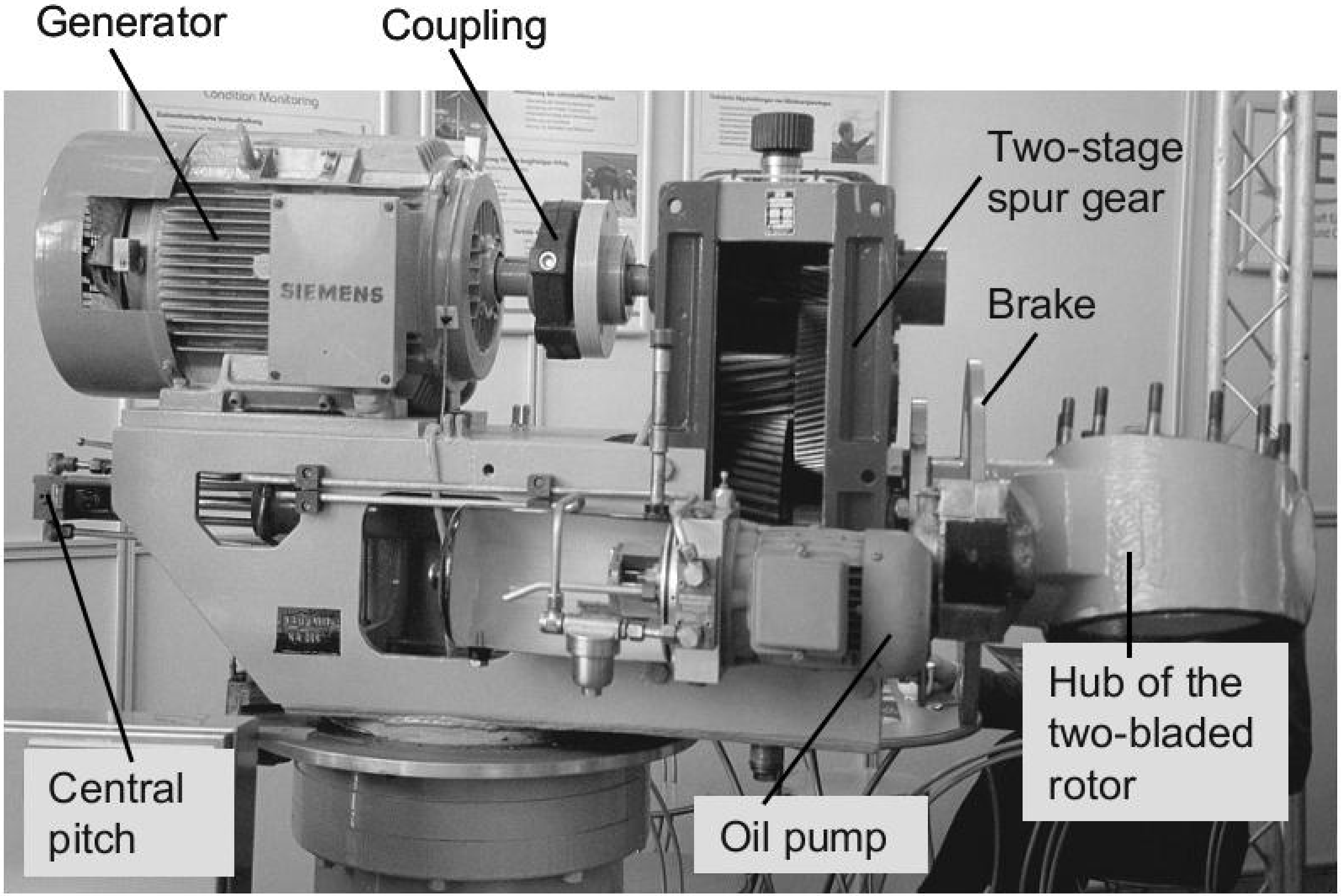

Fig. 3-38 Small wind turbine (two-bladed downwind rotor) with two-stage helical spur gear

Yaw system

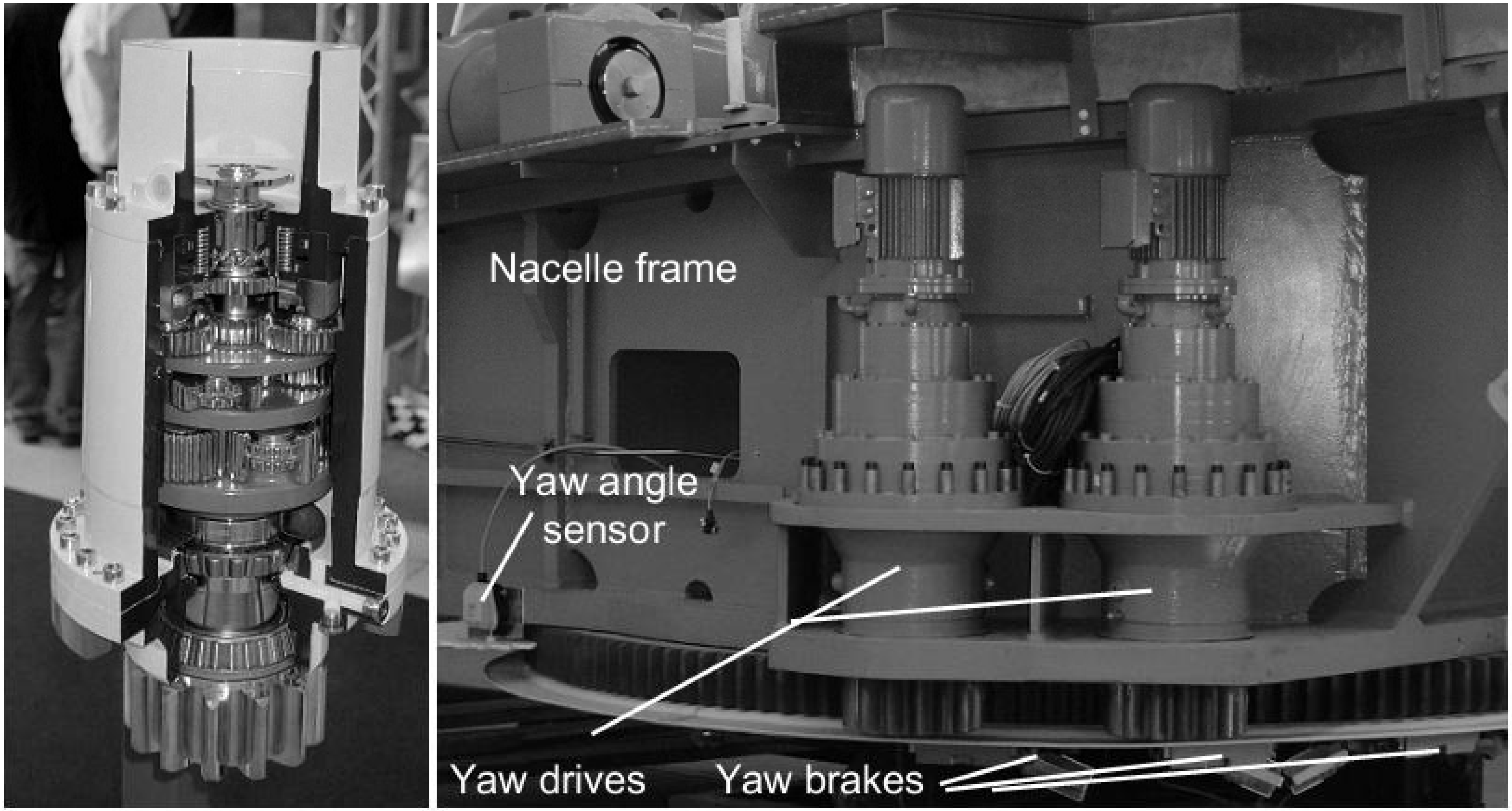

Fig. 3-45 Left: section of a yaw drive with multi-stage planetary gear, motor removed (Liebherr); right: electrical yaw drive, yaw brakes and yaw angle sensor (REpower)

Lightning protection

Fig. 3-47 Components of the lightning protection system for the protection of the bearings; left: sliding brush contact on the main shaft, right: on the yaw drive, combined with spark gaps (RE-power)

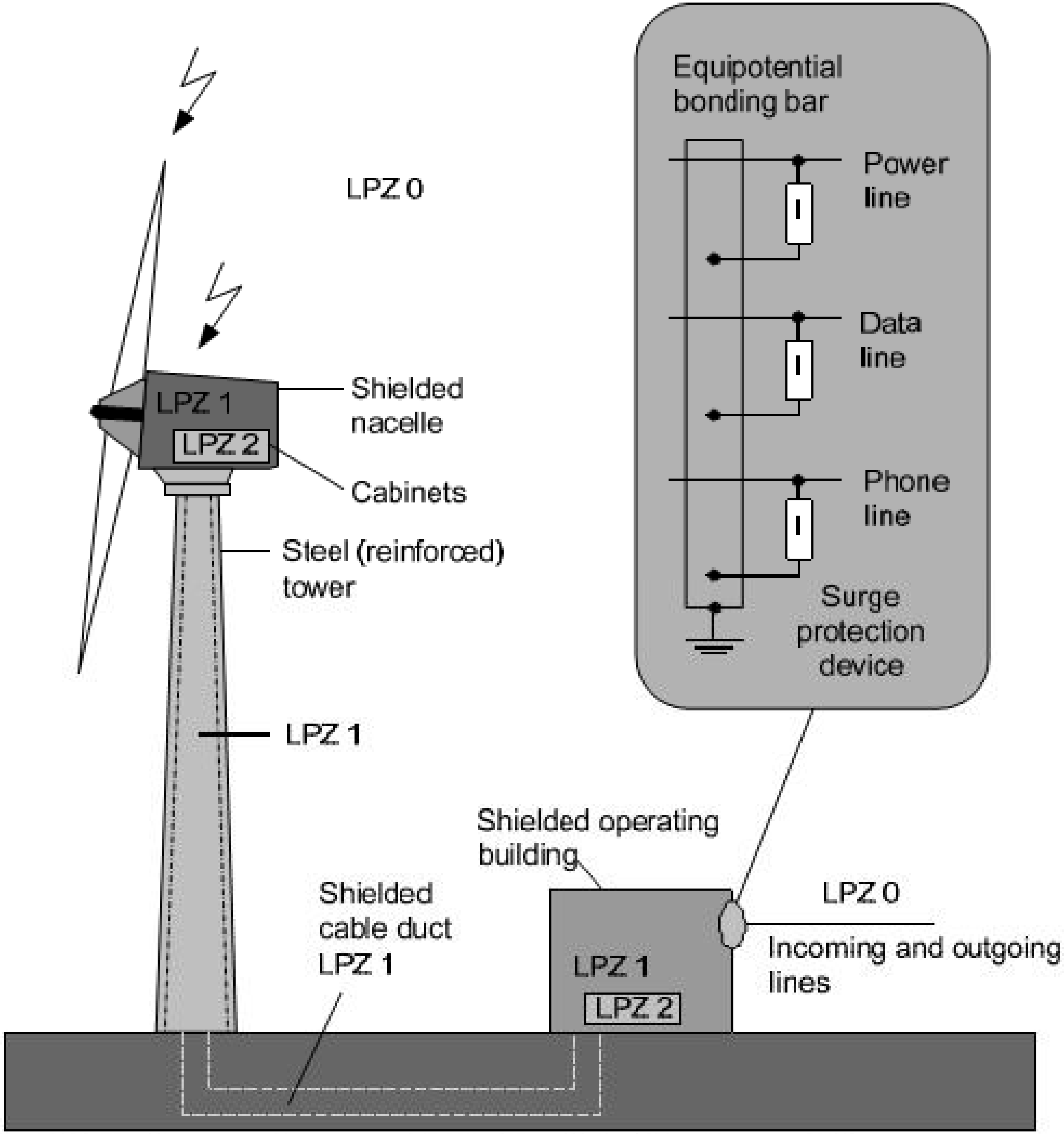

Fig. 3-48 Lightning protection zones (LPZ) of a wind turbine [acc. to 21]

Sensors

- Wind speed and direction
- Rotor and generator speed
- Temperatures (ambient, bearings, gearbox, generator, nacelle)
- Pressure (gearbox oil, cooling system, pitch hydraulics)
- Pitch and yaw angle
- Electrical data (voltage, current, phase)
- Vibrations and nacelle oscillation

Foundation

Fig. 3-59 Flat foundation